Science of the Total Environment 906 (2024) 167608

Contents lists available at ScienceDirect

Science of the Total Environment

journal homepage: www.elsevier.com/locate/scitotenv

# The role of snow in scavenging aerosol particles: A physical-chemical characterization

C. Blanco-Alegre [a,*], A.I. Calvo [a], A. Castro [a], F. Oduber [a], E. Alonso-Blanco [b], C. Alves [c], M. Cerqueira [c], R. López [d], F. Lucarelli [e], S. Nava [e], G. Calzolai [e], R. Fraile [a]

[a] Department of Physics, Universidad de León, Campus de Vegazana, 24071 León, Spain
[b] Centre for Energy, Environment and Technology Research (CIEMAT), Environment Department, Madrid, Spain
[c] Centre for Environmental and Marine Studies (CESAM), Department of Environment and Planning, University of Aveiro, Aveiro 3810-193, Portugal
[d] Department of Chemistry, Universidad de León, Campus de Vegazana, 24071 León, Spain
[e] Department of Physics and Astronomy, University of Florence and INFN-Florence, Florence, Italy

## HIGHLIGHTS

- Scavenging caused by snow was studied using spectrometer and disdrometer measurements.
- An effective washing of particles was observed during the first 30 min of snowfall.
- An increase of aerosol concentration in all modes was registered after snowfall.
- The chemical species with the highest scavenging values were $Mg^{2+}$, $Na^{+}$ and $Cl^{-}$.
- The events without effective washing showed high insoluble and low soluble carbon.

## GRAPHICAL ABSTRACT

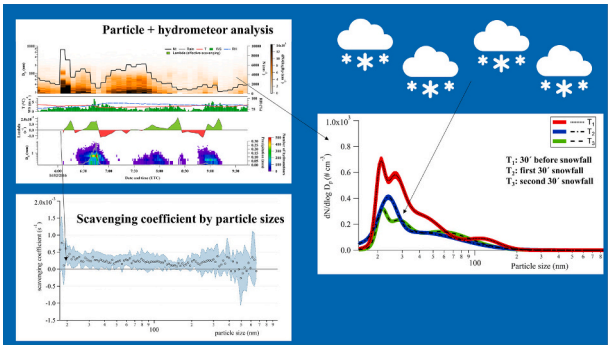


## ARTICLE INFO

Editor: Anastasia Paschalidou

*Keywords:*
Aerosol size distributions
Below cloud scavenging
Disdrometer
Scavenging coefficient
Snowflakes

## ABSTRACT

The below cloud scavenging of aerosols by snow has been analysed in León (NW Spain). Six snow events were registered over the course of one year of study. Ultrafine and accumulation aerosol particles were measured using a scanning mobility particle sizer spectrometer, while hydrometeors were characterized using a disdrometer. Furthermore, the chemical composition of the melted snow-water samples (soluble and insoluble fractions) was analysed.

The scavenging coefficient ($\lambda$) showed a great variability among events. An effective washing of particles was observed during the first 30 min of snowfall. The mean change in the scavenging efficiency ($\%\Delta C$) of particle number concentration (PNC) and $\lambda$ coefficient during this time interval were: i) nucleation mode: 36.3 % and $3.02 \cdot 10^{-4}$ $s^{-1}$; ii) Aitken mode: 30.4 % and $2.37 \cdot 10^{-4}$ $s^{-1}$ and iii) accumulation mode: 22.4 % and $1.77 \cdot 10^{-4}$ $s^{-1}$. The range of particle sizes that is less efficiently scavenged by snowfall was observed between 400 and 600 nm. When analyzing the whole snow event, an increase of PNC was observed. Two possible explanations underlie this behaviour: it could be caused by changes in air masses or by the resuspension of aerosol particles scavenged by snowflakes upon reaching the ground. A clear relationship was observed between $Ca^{2+}$, $SO_4^{2-}$ and $NO_3^{-}$

* Corresponding author.
*E-mail address:* cblaa@unileon.es (C. Blanco-Alegre).

https://doi.org/10.1016/j.scitotenv.2023.167608
Received 28 July 2023; Received in revised form 2 October 2023; Accepted 3 October 2023
Available online 5 October 2023

concentrations of aerosol particles before the snow event and the concentrations registered in the melted snow-water.

The largest and smallest changes in aerosol number concentrations were caused by snowflakes of 3 and 6 mm in diameter, respectively. The particle size distributions (PSD) were fitted to log-normal distributions and the parameters were compared before and after snowfall.

## 1. Introduction

Atmospheric aerosol particles influence climate inasmuch as absorb or reflect radiation and modify cloud properties (Fuzzi et al., 2015; Rosenfeld et al., 2014). Furthermore, aerosols influence human health since they are related to respiratory and cardiovascular diseases (Dockery et al., 2007; Tang et al., 2017), mainly affecting children (UNICEF, 2016).

The dynamic of aerosol concentrations is strongly controlled by the removal rates from the atmosphere. Wet deposition is the most important cleansing mechanism of aerosol particles. It can be divided into below-cloud (BCS) and in-cloud scavenging (ICS). BCS depends on the hydrometeor size distribution and precipitation intensity. Although several advances have been achieved in the last years, BSC is still a challenge due to its complexity (Andronache et al., 2006; Chate et al., 2011; Pryor et al., 2016; Zikova and Zdimal, 2016). This mechanism is caused by several processes, such as Brownian diffusion, interception, inertial impaction, thermophoresis, among others (Andronache et al., 2006; Lemaitre et al., 2020).

In recent years, numerous articles about the scavenging of aerosol particles by rain have been published (Andronache, 2003; Blanco-Alegre et al., 2021, 2019; Slinn, 1983; Zikova and Zdimal, 2016). However, scavenging caused by snow has been less studied (Kyrö et al., 2009; Lei and Wania, 2004; Paramonov et al., 2011; Radke et al., 1980), particularly in the south of Europe. There is a need to improve the schemes by conducting further research on BCS caused by snow, as noted by Jones et al. (2022). The aerosol particle size distributions during snow events are rarely reported (Zikova and Zdimal, 2016) and unprecedented in the Iberian Peninsula. Zikova and Zdimal (2016) found a low number of particles in the nucleation mode during snowfall, probably related to the scavenging caused by snowflakes and the filtering effect of the holes in the snowflakes (Mitra et al., 1990). The study carried out by Illuminati et al. (2016) in Antarctica showed a different scavenging depending on the aerosol size. They found that the scavenging caused by snowfall explained a decrease of 80 % of the coarse fraction (between 3 and 10 μm).

Scavenging of aerosol particles by snowflakes is more complicated than by raindrops due to the irregular shape of ice elements (Levin, 2009). It causes large uncertainties in the values of collection efficiency between experimental results and theoretical models, especially for submicron particles. Linked to this, most studies have shown that falling snow is a more efficient scavenger of air particles than rain due to its higher porosity (Franz and Eisenreich, 1998). Some theoretical BCS models corroborate this fact, although they show some uncertainties in the terminal velocity, cross-section, snowflake size and collision efficiency between aerosols and snowflakes (Croft et al., 2009; Feng, 2009). Furthermore, Lei and Wania (2004) found that snow is a better scavenger of organic chemicals than rain, although it depends on temperature. However, the snow scavenging coefficients for aerosol particles present a great variability among studies, from $1.9 \cdot 10^{-6}$ to $4.2 \cdot 10^{-5}$ $s^{-1}$ in Helsinki, Finland (Paramonov et al., 2011) or from $3.1 \cdot 10^{-7}$ to $1.2 \cdot 10^{-3}$ $s^{-1}$ in Lanzhou, China (Zhao et al., 2015).

After the snowflakes have fallen to the ground and melted, the aerosol particles incorporated into them can be transferred to the ground causing major impacts (Kang et al., 2020), remain in the meltwater (Meyer and Wania, 2011, 2008), or return to the atmosphere (Ariya et al., 2011). Pousse-Nottelmann et al. (2015) reported an increase in Aitken, accumulation and coarse modes after deposition of snowflakes on the ground (after removal of aerosols from the atmosphere).

Thus, does the intensity and duration of snowfall, or snowflake size affect the aerosol scavenging process? To address this question, several snow events will be thoroughly characterized, including aerosol particle size distribution (PSD) before, during and after snowfall, snowflake sizes and meteorological variables. Also, the chemical composition of some melted snow samples will be analysed.

## 2. Methodology

### 2.1. Sampling site

León (42°36′N, 05°35′W) is a Spanish city with a population of about 200,000 inhabitants located in the northwest of the Iberian Peninsula at an altitude of 838 m above sea level. Based on the records of the last 35 years, León presents an annual mean temperature of 11.1 °C, 13 snowy days and 75 rainy days, with a total mean precipitation of 515 mm mainly concentrated in winter and spring (data provided by the Spanish Meteorological Agency (http://www.aemet.es)). The sampling campaign was conducted between 12 February 2016 and 14 March 2017. The instruments were located in the Faculty of Veterinary Medicine of the University of León. In winter, the major sources of aerosol particles are traffic and domestic heating devices, since large emitting industries do not directly affect the site (Blanco-Alegre et al., 2019; Oduber et al., 2021a).

### 2.2. Snow event selection

The beginning of the snowfall event is defined as the minute in which a precipitation volume of at least 0.01 mm is recorded. The end of the event is considered when the precipitation is <0.01 mm for 15 min. Selected snow events have fulfilled the following requirements: i) no missing particle or meteorological data; ii) a minimum of 60 precipitation-free minutes between events; iii) variations in temperature, relative humidity and wind speed below ±3.5 °C, ±25 % and 2 m $s^{-1}$, respectively, within 30 min before and after precipitation to avoid changes caused by meteorological factors outside snow (Hussein et al., 2006). Other authors have used similar criteria to avoid the influence of hygroscopic aerosol growth and meteorology on scavenging (Blanco-Alegre et al., 2021; Kyrö et al., 2009; Zhao et al., 2015). In León during sampling, a total of six snow events were found to satisfy the criteria that were previously mentioned.

### 2.3. Particle sampling

The ultrafine (UFP) and accumulation aerosol particles were measured using a scanning mobility particle sizer spectrometer (SMPS Model 3938, TSI, Minnesota, USA). The aerosol sample flow passes through a Nafion dryer incorporated at the inlet that dries aerosol to or below 40 % relative humidity (Wiedensohler et al., 2012). The flow ratios were 0.3 and 3 L $min^{-1}$ for the aerosol sample and sheath flow, respectively. This configuration provided a complete size distribution between 14.3 and 1000 nm in 110 channels with a temporal resolution of 6 min. Multiple charge and diffusion corrections in the line and system were applied according to the ACTRIS SMPS standards (Wiedensohler et al., 2012). During each snowfall, the real-time particle number concentration (PNC) and PSD were fitted to normal distribution through the sum of two or three lognormal distributions.

PNC at each size bin was corrected using the daily pattern of the periods without precipitation covering the 15 days before and after the snowfall, following the methodology shown in Blanco-Alegre et al. (2018). The daily pattern used to correct each event is shown in Fig. A1.

$PM_{10}$ sampling was carried out with a low-volume sampler (Echo PM, TECORA, Cogliate, Italy) that collected the aerosol mass on teflon filters (Ø = 47 mm) and a high-volume air sampler (CAV-A/Mb model, MCV, Barcelona, Spain) that collected the aerosol mass on quartz filters (Ø = 150 mm).

### 2.4. Hydrometeors sampling and meteorological parameters

To characterize the snowflakes, a disdrometer Laser Precipitation Monitor (LPM) of Thies Clima (Göttingen, Germany) has been used. It registers hydrometeors between 0.125 and 8 mm in 22 channels. The following precipitation variables, on one-minute basis, were obtained: terminal velocity (m $s^{-1}$), precipitation intensity (mm $h^{-1}$), accumulated precipitation (mm), number of hydrometeors in each channel ($m^{-3}$), water content (total volume of hydrometeors per cubic metre ($mm^3$ $m^{-3}$)), swept volume by falling hydrometeors for each size bin ($mm^3$ $m^{-3}$) and average of the snowflake sizes (mm). Swept volume and terminal velocity were estimated following the methodology described by Blanco-Alegre et al. (2021). The estimated relative error of the parameters calculated using this method is <18 %. It is important to highlight that the accuracy of snowflake diameter measurements can also be influenced by their shape, potentially leading to discrepancies of <20 % in the measurements obtained from the optical disdrometer (Battaglia et al., 2010).

Snow-water samples were collected in glass bottles using a rainwater collector (UNS 130/E, Eigenbrodt, Königsmoor, Germany). Every bottle was sampled for a period of 23.5 h (≈1 day), from 1000 to 0930 UTC. Furthermore, a Davis weather station (Hayward, USA) continuously registered the temperature (T), relative humidity (RH), wind speed (WS) and wind direction (WD). Planetary Boundary Layer (PBL) height was obtained from data made available by the National Oceanic and Atmospheric Administration (NOAA) (https://www.ready.noaa.gov/READYamet.php).

### 2.5. Analytical methodologies

The chemical composition of the melted snow-water samples was analysed. The conductivity and pH were determined after collection with a Hach, HQ 40d multi metre (Manchester, United Kingdom). Then samples were filtered through a quartz filter (Ø = 25 mm) in order to separate the insoluble and soluble fractions. The soluble fraction was analysed for i) t dissolved organic carbon (DOC) by combustion and infrared detection in a Total Organic Carbon Analyzer (TOC-VCPH, Shimadzu, Duisburg, Germany) and ii) water soluble inorganic ions using a Thermo Scientific Dionex™ ICS-5000 equipment (Massachusetts, USA) equipped with an IonPac® CS16 column (4 × 250 mm) for the analysis of cations ($Na^+$, $K^+$, $Ca^{2+}$, $Mg^{2+}$ and $NH_4^+$) and an IonPac® AS11 column (4 × 250 mm) for the analysis of anions ($F^-$, $Cl^-$, $SO_4^{2-}$, $NO_3$ and $NO_2^-$). Furthermore, the quartz filters, containing the insoluble fraction, were analysed for organic and elemental carbon (WIOC and WIEC, respectively) using a thermo-optical technique (Custódio et al., 2014; Pio et al., 2011).

The aerosol chemical composition was obtained from the analysis of daily $PM_{10}$ filter samples collected during the same sampling campaign (AERORAIN project). Quartz filters were used to determine $PM_{10}$ by gravimetry on an electronic semi-microbalance (XPE105DR, Mettler Toledo, Ohio, USA) (with a precision of 0.00001 g), and organic and elemental carbon, using a thermo-optical technique (Alves et al., 2015; Pio et al., 2011). Teflon filters were used to determine major trace elements by Particle-Induced X-ray Emission (PIXE) (Lucarelli et al., 2015).

### 2.6. Parameters of scavenging

After selecting the snow events, the scavenging efficiency (%$\Delta C$) and the scavenging coefficient ($\lambda$) have been determined (Eqs. (1) and (2); Seinfeld and Pandis, 2016). For each snowfall, 4 periods were defined as follows:

- T1: half an hour before the start of the snowfall.
- T2: first half hour after the start of the snowfall. For one of the studied events, $T_2$ was shorter than 30 min due to the short-term duration of the event (lower than 30 min).
- T3: second half hour after the start of the snowfall.
- T4: half an hour after the end of the snowfall.

To eliminate the eventual influence of external sources of particles, the scavenging effect caused by snowflakes has been evaluated during two consecutive periods of 30 min from the beginning of the snowfall ($T_2$ and $T_3$, respectively). Thus, %$\Delta C$ and $\lambda$ ($s^{-1}$) have been calculated considering the aerosol concentration data:

- registered during the first 30 min ($T_2$) or 30 min after snowfall ($T_4$) compared with the concentration recorded 30 min before snowfall ($T_1$). The comparison $T_1$-$T_4$ is the "entire event evaluation".

- the second 30 min ($T_3$) of snow precipitation will be also used to analyze the evolution of scavenging throughout the event, in comparison with the mean concentration registered during the time period $T_2$.

- in order to analyze the evolution of %$\Delta C$ and $\lambda$, the one-minute aerosol concentration registered during snowfall was compared with the mean concentration registered in the previous 30 min.

$$\%\Delta C = -\left(\frac{C_b - C_a}{C_a}\right)\cdot 100 \tag{1}$$

$$\lambda\left(d_p\right) = -\frac{1}{t_b - t_a}\cdot ln\left(\frac{C\left(d_p\right)_b}{C\left(d_p\right)_a}\right) \tag{2}$$

where $d_p$ is the aerosol particle diameter (nm) and $C$ is the aerosol concentration ($cm^{-3}$). The subscripts $a$ and $b$ represent any time interval T1, T2, T3 or T4, $b$ being later than $a$.

Likewise, %$\Delta C$ and $\lambda$ were estimated every 10 min for the nucleation mode (particle sizes <30 nm) ($\lambda_{nuc}$ and %$\Delta C_{nuc}$), Aitken mode (particle sizes between 30 and 100 nm) ($\lambda_{Ait}$ and %$\Delta C_{Ait}$), accumulation mode (particle sizes between 100 and 1000 nm) ($\lambda_{acc}$ and %$\Delta C_{acc}$) and for the total aerosol particles ($\lambda_{global}$ and %$\Delta C_{global}$). Positive values of %$\Delta C$ and $\lambda$ are indicative of effective scavenging.

The scavenging coefficients for ionic species ($W$) have been calculated following the methodology indicated by Oduber et al. (2021b) (Eq. (3)).

$$W = \frac{C_{snow}}{C_{air}}\cdot\frac{\rho_{air}}{\rho_{snow}} \tag{3}$$

where $C_{snow}$ is the concentration of the ionic species in mg $L^{-1}$ in snow samples, $C_{air}$ is the concentration of the same species in μg $m^{-3}$ in the air, $\rho_{air}$ is the air density ($1.29 \times 10^9$ μg $m^{-3}$) and $\rho_{snow}$ is the snow density ($10^{12}$ μg $m^{-3}$).

Furthermore, the volume-weighted mean concentrations (VWM) of ionic species (μeq $L^{-1}$) were calculated using Eq. (4)

$$VWM = \frac{\sum_{i=1}^{N} C_i S_i}{\sum_{i=1}^{N} C_i} \tag{4}$$

where $C_i$is the concentration in μeq $L^{-1}$, $S_i$ is the precipitation accumulated (mm) for each snow event and $N$ the total number of snow events.

### 2.7. Air mass origin

The origin of air masses during snow events was obtained using the HYSPLIT4 (Hybrid Single Particle Lagrangian Integrated Trajectory) NOAA model (Draxler and Rolph, 2012) based on four-days back trajectories at 1000 m a.g.l. over the sampling point. Two trajectories for each day, at 0000 and 1200 UTC, were obtained. The methodology was the same as in Blanco-Alegre et al. (2019), with a classification into six categories: Arctic, Atlantic Ocean, Continental European, North America, North Atlantic Ocean and Saharan desert. The model was run with meteorological data from the Global Data Assimilation System (GDAS) archives (http://ready.arl.noaa.gov/HYSPLIT_traj.php).

## 3. Results and discussion

### 3.1. Characterization of events

The six snowfalls that meet the aforementioned criteria were concentrated in the winter months (January and February). A wide range of accumulated snow-water values was registered (Table 1), with a minimum of 0.9 mm (Event E6) and a maximum of 66.4 mm (E2). Two different groups were established based on the intensity of precipitation: intensities lower than 1 mm $h^{-1}$ (E1, E3 and E6) and intensities higher than 4 mm $h^{-1}$ (E2, E4 and E5). The maximum snow intensity during $T_2$ was registered in the E5 (7.39 mm $h^{-1}$) and E3 (2.14 mm $h^{-1}$), while the remaining events presented snow intensities lower than 0.5 mm $h^{-1}$.

Mean temperature and relative humidity were similar during all events, ranging between 0.86 and 2.67 °C and between 78.3 and 87.2 %, respectively. As mean temperatures were above 0 °C, the ice particles could have partially melt and reach the ground as wet snow (Levin, 2009). However, the mean wind speed differed between events, with a minimum of 0.13 m $s^{-1}$ (E3) and a maximum of 7.51 m $s^{-1}$ (E5), but the difference between before and after was lower than 2 m $s^{-1}$ (Section 2.5). As expected, meteorological parameters analysed during $T_2$ are very similar to those of the global event, with a mean wind speed ranging from 0.08 m $s^{-1}$ (E3) to 6.57 m $s^{-1}$ (E5).

An increase in PBL height was recorded between before and after snowfall due to events starting at night or in early morning (except in E3 and E6, during which an intense atmospheric thermal inversion was registered, with PBL height values lower than 100 m). The PBL height is key to the evolution of pollutant concentrations at the surface (Su et al., 2018), so a higher PBL height after the snowfall favors the decrease of aerosol concentrations. The combined influence of the higher PBL height and the scavenging effect of snowfall contributes to the overall reduction of aerosol concentrations near the surface. However, despite these insights, the precise significance of each factor requires further in-depth analysis.

The origin and transport pathways of air masses reaching the sampling point during the snow events can be observed in Fig. 1. North America origin is the most common class (E4, E5 and E6 with a mean PNC before snow of 172, 1074 and 2142 $cm^{-3}$, respectively), while North Atlantic Ocean (E1 with a mean PNC of 4148 $cm^{-3}$), Continental European (E2 with a mean PNC of 1392 $cm^{-3}$) and Saharan desert (E3 with a mean PNC of 2165 $cm^{-3}$) provenances represented one case each. The typical particle number size distribution depending on the air mass origin arriving at León are presented in Blanco-Alegre et al. (2022), mainly pointing out that Continental and Saharan origins showed the highest number concentration of aerosol particles with diameters higher than 65 nm. Size distributed PNC showed clear differences among events, with higher number of particles in E1, E3 and E6 (Table 2). E3 showed distinctive characteristics, as it was a snow event after a Saharan dust intrusion (Oduber et al., 2019), and it showed a different PSD than the rest of the events (Fig. 2) with a high number of particles larger than 100 nm.

In all snowfall cases studied, the synoptic situation at ground level indicates that low pressures were registered over the Iberian Peninsula.

**Table 1**
Summary of snowfall characteristics and mean meteorological parameters.

| Event | Date | Evaluation of the entire event | | | | | | | | | First time interval ($T_2$) from the beginning of the snow event | | | | | | | | |
|---|---|---|---|---|---|---|---|---|---|---|---|---|---|---|---|---|---|---|---|
| | | Start (UTC) | End (UTC) | Duration (hh:mm) | Snow accumulated (mm) | Intensity (mm $h^{-1}$) | T (°C) | RH (%) | Wind (m $s^{-1}$) | PBL before (m) | PBL after (m) | Start (UTC) | End (UTC) | Duration (hh:mm) | Snow accumulated (mm) | Intensity (mm $h^{-1}$) | T (°C) | RH (%) | Wind (m $s^{-1}$) |
| E1 | 14/02/2016 | 6:24 | 9:13 | 2:36 | 2.4 | 0.84 | 2.67 | 86.1 | 1.92 | 293 | 1026 | 6:24 | 6:54 | 0:30 | 0.25 | 0.49 | 2.90 | 83.9 | 2.59 |
| E2 | 15/02/2016 | 1:06 | 14:59 | 13:53 | 66.4 | 4.78 | 1.60 | 87.2 | 2.41 | 632 | 1386 | 1:06 | 1:36 | 0:30 | 0.13 | 0.26 | 2.52 | 79.5 | 2.63 |
| E3 | 02/01/2017 | 4:14 | 6:15 | 2:01 | 1.6 | 0.77 | 0.86 | 84.8 | 0.13 | 96 | 78 | 4:14 | 4:44 | 0:30 | 1.07 | 2.14 | 0.89 | 82.3 | 0.08 |
| E4 | 05/02/2017 | 6:07 | 10:50 | 4:43 | 27.7 | 5.87 | 1.39 | 86.8 | 3.59 | 1375 | 1646 | 6:07 | 6:37 | 0:30 | 0.06 | 0.13 | 2.00 | 77.9 | 4.54 |
| E5 | 05/02/2017 | 12:21 | 12:37 | 0:16 | 2.0 | 7.39 | 2.64 | 78.3 | 7.51 | 1646 | 2192 | 12:21 | 12:37 | 0:16 | 1.97 | 7.39 | 2.45 | 80.5 | 6.57 |
| E6 | 10/02/2017 | 5:41 | 7:18 | 1:37 | 0.9 | 0.57 | 1.51 | 79.8 | 0.70 | 89 | 70 | 5:41 | 6:11 | 0:30 | 0.14 | 0.27 | 1.74 | 71.4 | 0.80 |

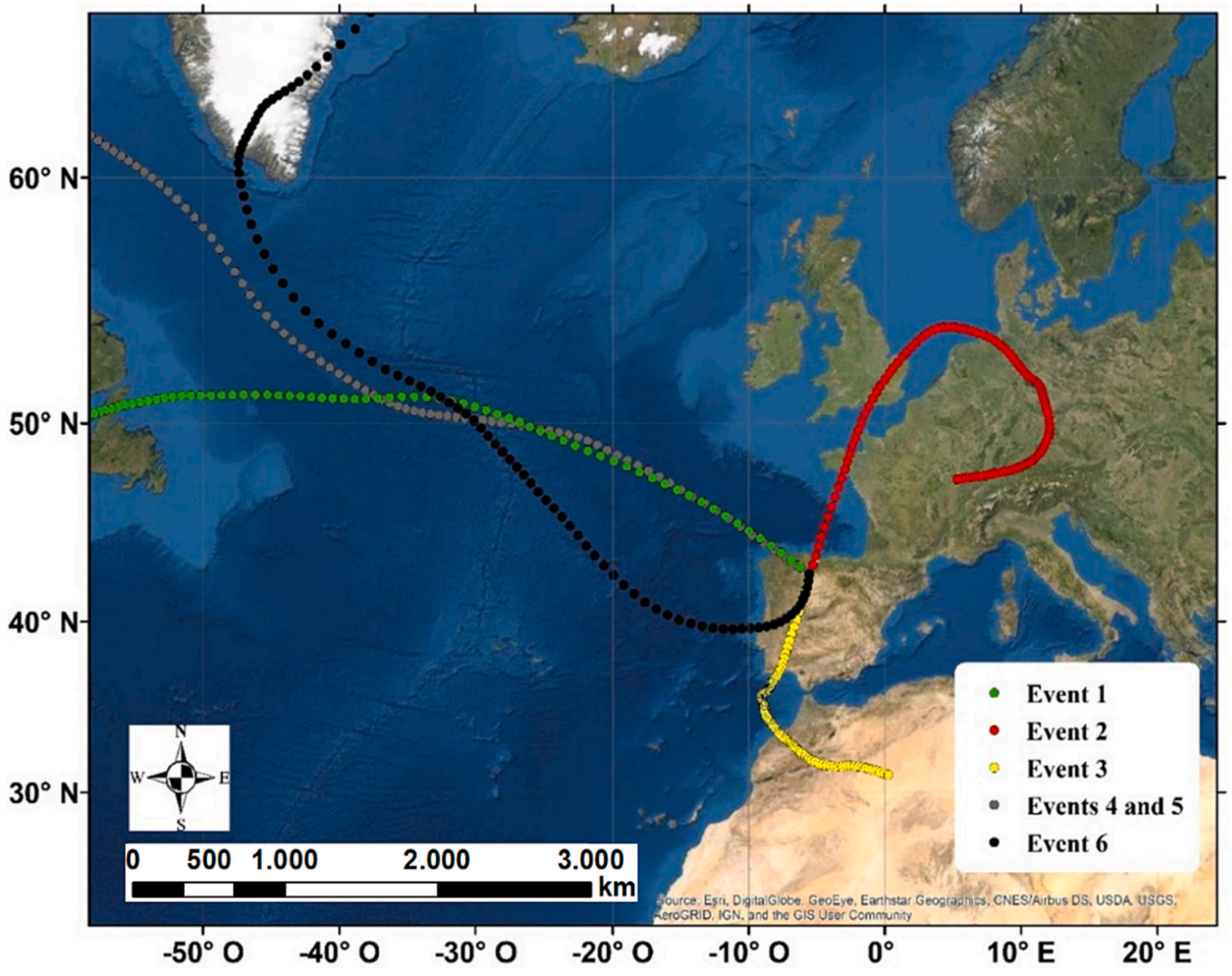


**Fig. 1.** Four-days back trajectories (1000 m a.g.l.) arriving in León during snow events.

**Table 2**
Mean PNC (corrected by daily pattern) during $T_1$ and $T_2$, scavenging coefficient and scavenging efficiency ($\%\Delta C$) for nucleation (14–30 nm), Aitken (30–100 nm), accumulation (100–1000 nm) and global (14–1000 nm) modes.

| Event | $PNC_{nuc\ 1}$ ($cm^{-3}$) | $PNC_{nuc\ 2}$ ($cm^{-3}$) | $\lambda_{nuc}$ ($10^{-5}\ s^{-1}$) | $\%\Delta C_{nuc}$ | $PNC_{Ait\ 1}$ ($cm^{-3}$) | $PNC_{Ait\ 2}$ ($cm^{-3}$) | $\lambda_{Ait}$ ($10^{-5}\ s^{-1}$) | $\%\Delta C_{Ait}$ | $PNC_{acc\ 1}$ ($cm^{-3}$) | $PNC_{acc\ 2}$ ($cm^{-3}$) | $\lambda_{acc}$ ($10^{-5}\ s^{-1}$) | $\%\Delta C_{acc}$ | $PNC_{global1}$ ($cm^{-3}$) | $PNC_{global2}$ ($cm^{-3}$) | $\lambda_{global}$ ($10^{-5}\ s^{-1}$) | $\%\Delta C_{global}$ |
|---|---|---|---|---|---|---|---|---|---|---|---|---|---|---|---|---|
| E1 | 7885 | 4778 | 27.8 | 39.4 | 6191 | 3698 | 28.6 | 40.3 | 1036 | 729 | 19.5 | 29.6 | 14,019 | 8478 | 27.9 | 39.5 |
| E2 | 3241 | 1804 | 32.6 | 44.4 | 1590 | 776 | 39.9 | 51.2 | 428 | 229 | 34.8 | 46.5 | 4306 | 2286 | 35.2 | 46.9 |
| E3 | 619 | 598 | 2.0 | 3.5 | 2997 | 2832 | 3.1 | 5.5 | 3794 | 3766 | 0.4 | 0.7 | 8611 | 8292 | 2.1 | 3.7 |
| E4 | 277 | 167 | 27.9 | 39.5 | 335 | 278 | 10.5 | 17.2 | 177 | 170 | 2.2 | 3.9 | 739 | 593 | 12.2 | 19.7 |
| E5 | 1040 | 811 | 25.9 | 22.0 | 1820 | 1426 | 25.4 | 21.6 | 721 | 538 | 30.6 | 25.4 | 3416 | 2659 | 26.1 | 22.2 |
| E6 | 3141 | 972 | 65.2 | 69.0 | 5498 | 2951 | 34.6 | 46.3 | 1882 | 1348 | 18.5 | 28.4 | 10,056 | 5162 | 37.0 | 48.7 |

A cold front entered the Peninsula from the northwest in all cases, except in E3, the event with a Saharan air mass origin, but with an entry of cold air masses from high-latitude areas (Figs. A2 and A3). Winter Saharan dust outbreaks affecting the Iberian Peninsula during winter occur typically under anticyclonic conditions, with intense subsidence thermal inversions (Russo et al., 2020). This phenomenon was probably registered in E3 (the closest available radiosonde, in Santander -about 350 km NE of León-, showed a subsidence thermal inversion at 875 m a.g.l.) (Fig. A4).

### 3.2. Scavenging efficiency and coefficient

Table 2 includes size segregated PNC, $\lambda$ and $\%\Delta C$ values. As can be observed in Fig. 2, the $\lambda$ coefficient during the snowfall presented positive values (effective scavenging) at the beginning of the events. However, throughout the events, the scavenging coefficient showed fluctuations and, in some events (E2, E3, E4 and E6), the particle concentration was higher in $T_4$ (after snowfall) than in $T_1$. Thus, the evolution of the mean $\lambda$ coefficient during snowfall (Fig. 3) shows that after 25 min the scavenging efficiency decreases.

The comparison of $\%\Delta C$ and $\lambda$ values between $T_1$ and $T_2$ shows a decrease of the mean of $\%\Delta C$ (36.3 ± 22.1 % for nucleation, 30.4 ± 18.2 % for Aitken, 22.4 ± 17.3 % for accumulation and 30.1 ± 17.8 % for the total distribution) and of the $\lambda$ coefficient ($3.02 \cdot 10^{-4} \pm 2.03 \cdot 10^{-4}\ s^{-1}$ for nucleation, $2.37 \cdot 10^{-4} \pm 1.42 \cdot 10^{-4}\ s^{-1}$ for Aitken, $1.77 \cdot 10^{-4} \pm 1.42 \cdot 10^{-4}\ s^{-1}$ for accumulation and $2.34 \cdot 10^{-4} \pm 1.37 \cdot 10^{-4}\ s^{-1}$ for the total distribution). Data of this type for different latitudes can provide valuable information for building and improving models (Ryu and Min, 2022).

When comparing values of $T_1$ (before) and $T_4$ (after snowfall), the $\%\Delta C$ parameter presented positive values only in 3 events in nucleation mode (Table A1). In Aitken and accumulation modes, except for E1, the concentration after snowfall was equal (E5) or higher than before precipitation. The analysis of the entire event did not show an effective scavenging, except during E1.

In general, the values obtained in snow events were similar to those obtained in rain events (Blanco-Alegre et al., 2021). However, higher scavenging values caused by snow than by rain have been reported by other authors (Kyrö et al., 2009; Witkowska et al., 2015; Zikova and Zdimal, 2016), mainly at temperatures above −10 °C (Zhao et al., 2015). Furthermore, Paramonov et al. (2011) have found a strong dependence of aerosol-hydrometeor interaction with micrometeorological parameters during snowfalls. In this study, the snow events presented the best possible meteorological conditions to scavenge (Paramonov et al., 2011), with temperatures between 0.9 and 2.7 °C and high relative humidity with values between 78 and 87 %. However, when comparing PNC before and after snow, a decrease was not registered, contrary to what was observed in rainfall events (Blanco-Alegre et al., 2021, 2018) during the same sampling campaign. It may be related to the fact that after the snowflakes fall to the ground and melt, the aerosol particles incorporated could return into the atmosphere (Ariya et al., 2011). Additionally, the arrival of air masses with a higher aerosol load after the snowfall, could be another reason (Babu et al., 2016).

In order to identify the range of particle sizes that are less efficiently scavenged by snowfall, akin to Greenfield gap used in rain scavenging analysis (Greenfield, 1957), the $\lambda$ coefficient was calculated using the data during the first 30 min ($T_2$) and during the second 30 min ($T_3$) of precipitation (Fig. 3). Positive values (efficient scavenging) were obtained along all the size distribution, except between 400 and 600 nm (with negative values around 500 nm). Therefore, this interval corresponds to the less efficiently scavenged gap. From 30 to 300 nm, $\lambda$ values were constant around $2.5 \cdot 10^{-4}\ s^{-1}$. Various studies report different boundaries for the size range of the this gap during snow events in smaller particles, for example between 60 and 300 nm in diameter (Paramonov et al., 2011) or between 100 and 300 nm in diameter (Kyrö et al., 2009; Laakso et al., 2003). However, Radke et al. (1980) reported

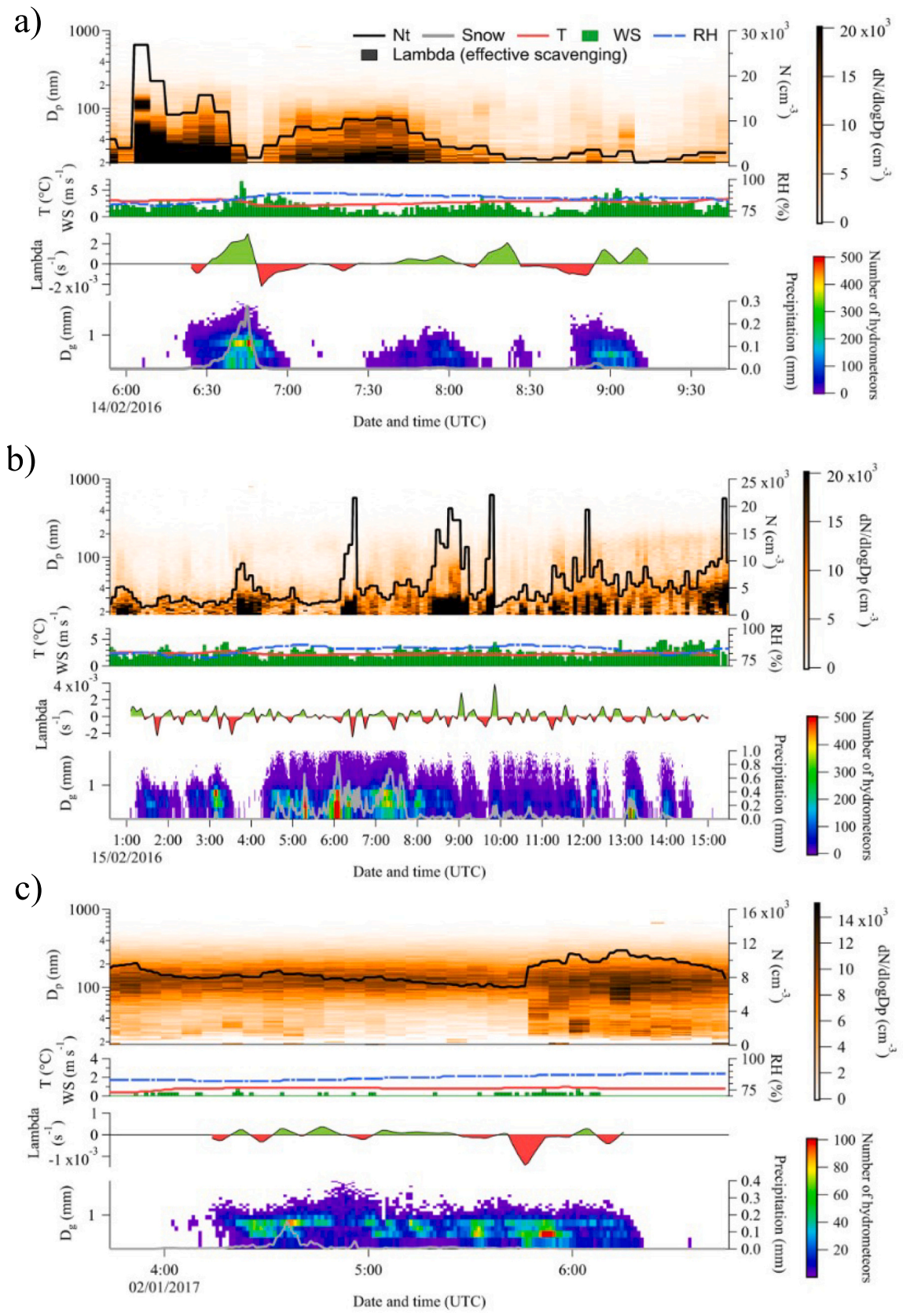


**Fig. 2.** Evolution of particle number concentrations (continuous black line), particle concentrations by sizes (in color scale); meteorological variables (T, RH and WS); scavenging coefficient ($\lambda$) (in red non-effective scavenging, in green effective scavenging) and snow-water accumulation (grey continuous line) and number of hydrometeors by sizes (in color) during events: a) E1; b) E2; c) E3; d) E4; e) E5 and f) E6.

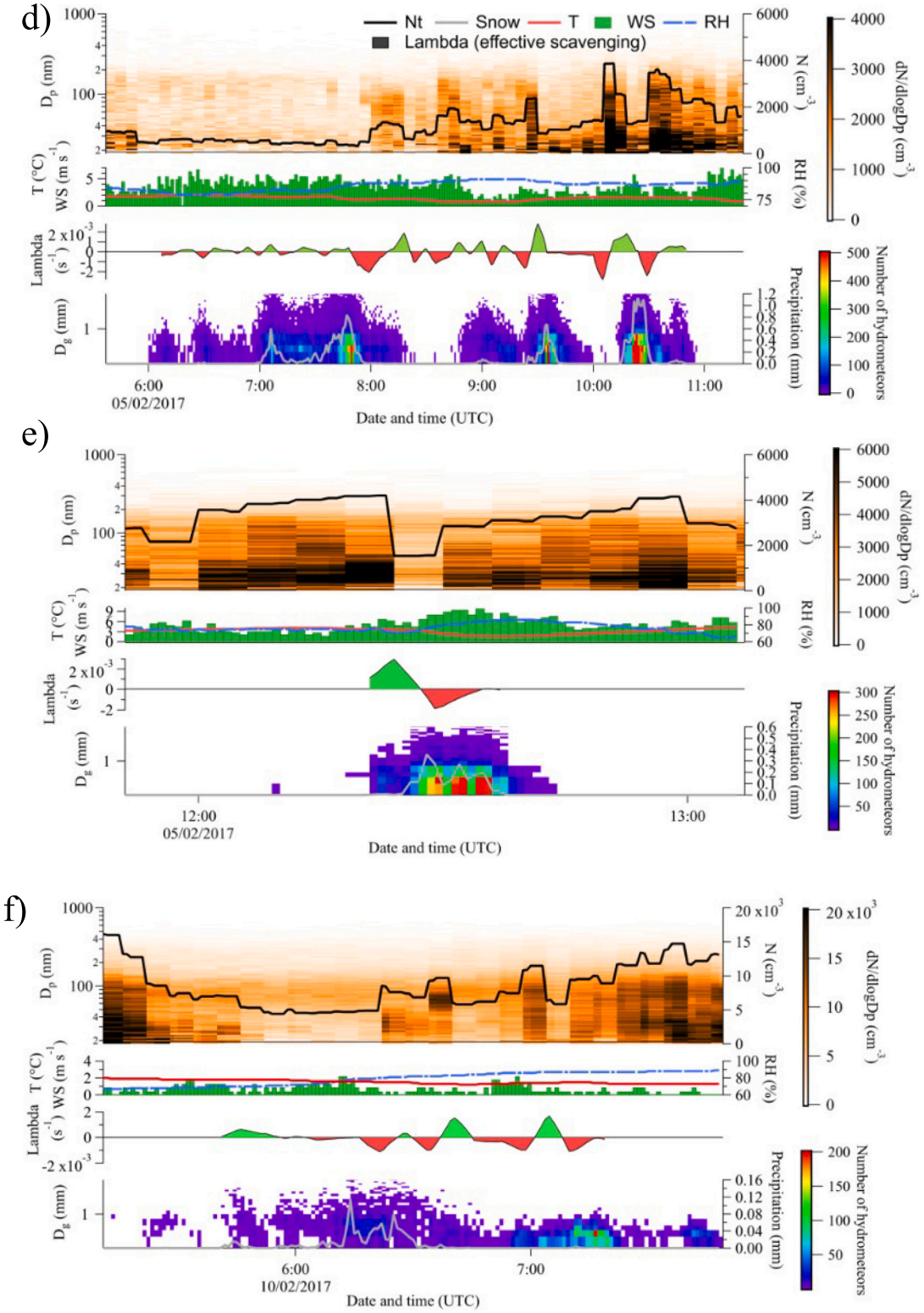


**Fig. 2.** (*continued*).

the less efficiently scavenged gap in larger sizes, around 1000 nm. These variations may be caused by the different snowflake sizes and water content of the snowflakes among studies, which affect the collision efficiency between hydrometeor and particle size (Andronache, 2003; Bae et al., 2006; Ladino et al., 2011).

In E1, E2 and E3, the swept volume was due to hydrometeors ranging between 0.125 and 4 mm, while in E4, E5 and E6 to hydrometeor sizes up to 7.5 mm with high swept volume values (Fig. A5). The Pearson correlation between the size-segregated snowflake number and $\%\Delta C$ every 10 min along events indicates positive values, so a higher number of hydrometeors caused a higher decrease in aerosol concentration. The maximum value was obtained for snowflake sizes of 3 mm ($p = 0.211$), while the minimum was obtained for 6 mm sizes ($p = 0.070$). It is remarkable that only E1 and E5 showed a significant correlation for all hydrometeor sizes. These events were the only ones with a lower particle concentration during $T_4$ than $T_1$.

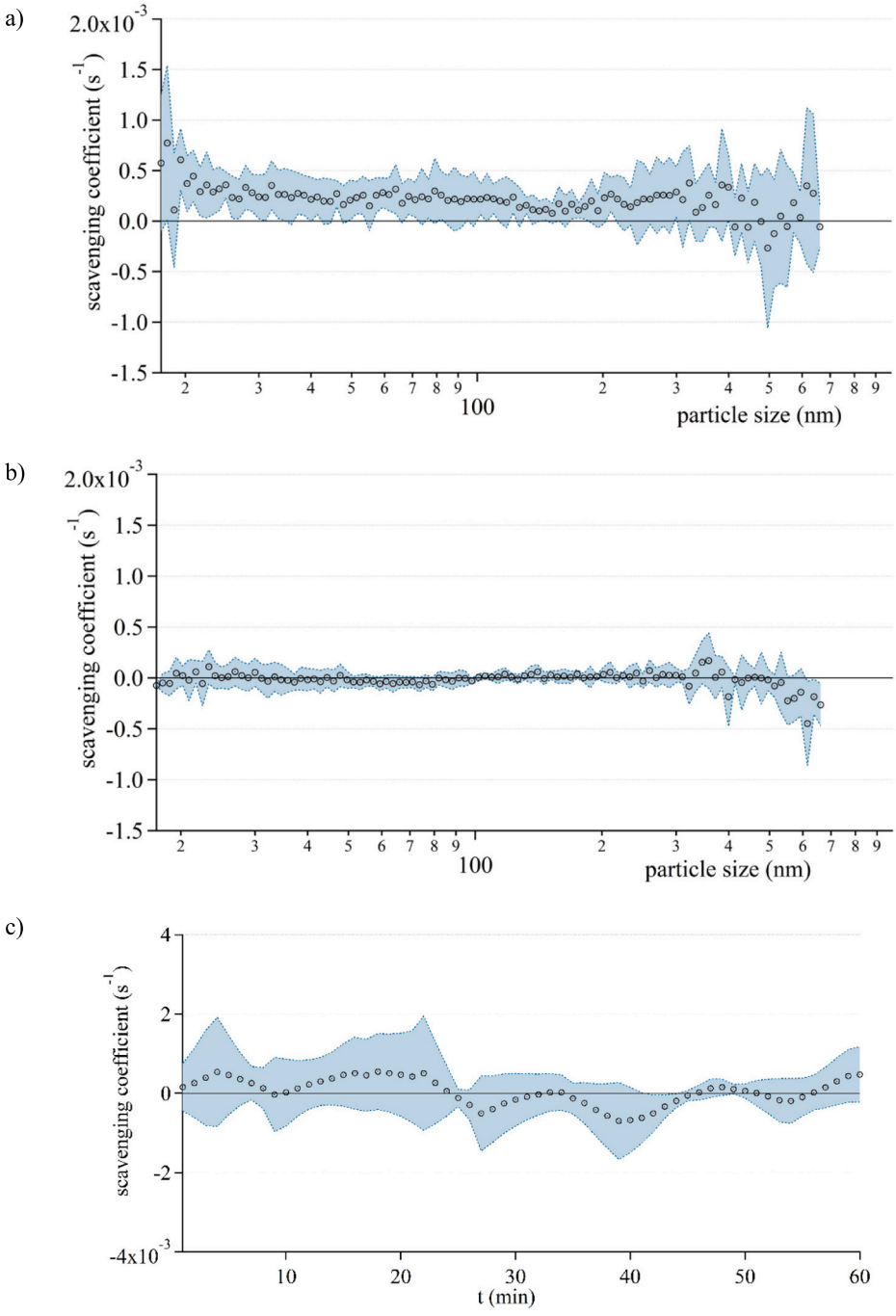


**Fig. 3.** Mean scavenging coefficient ($\lambda$) obtained for each SMPS channel during: a) $T_2$; b) $T_3$ and c) evolution of global $\lambda$ value during the first 60 min of snowfall. The dotted lines filled represent mean ± standard deviation value.

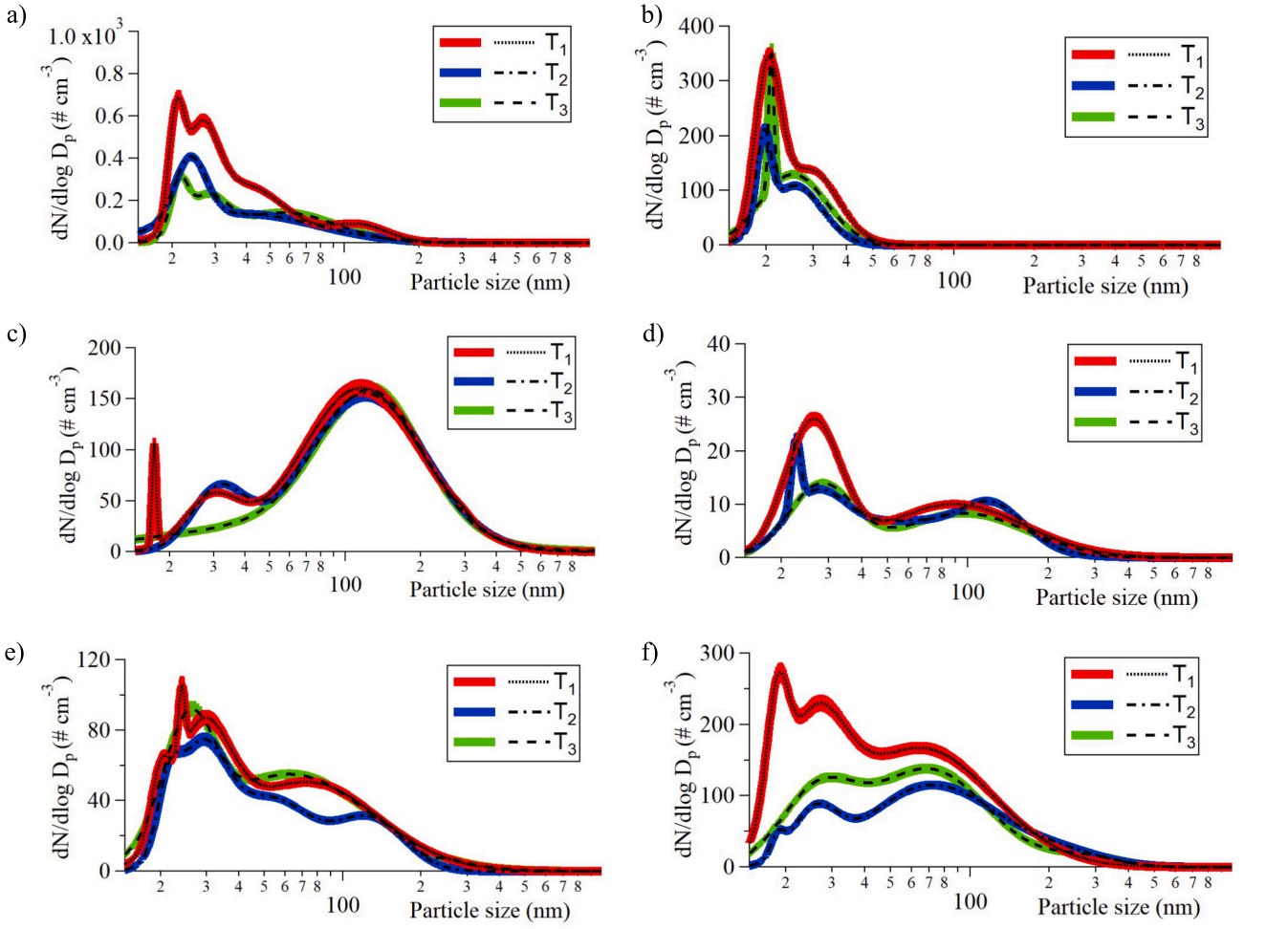


**Fig. 4.** Evolution of PSD before the snowfalls ($T_1$), during the first 30 min ($T_2$) and during the second 30 min ($T_3$) of snow: a) E1; b) E2; c) E3; d) E4; e) E5 and f) E6.

### 3.3. Evolution of particle size distributions

Contrary to rain events (Blanco-Alegre et al., 2021), the PSD in snowfalls presented a multimodal distribution (three or more peaks) (Fig. 4). Most of the scavenging caused by snow occurred in $T_2$, while in $T_3$ there were slight increases or decreases.

Table A2 shows the fit parameters for the log-normal distribution, where $D$ is the diameter, $\sigma$ is the amplitude (width parameter) and $N$ is the aerosol particle concentration (Jonasz and Fournier, 1996). A decrease in particle concentration is observed along all particle sizes when comparing the distributions before snowfall ($T_1$) and during $T_2$. Fig. A6 includes two examples of reconstructed model fitting.

In the nucleation peaks, E1 and E3 presented a decrease in the number of particles, both in $T_2$ and $T_3$ (no differences were detected between both periods). In general, $T_3$ showed a decrease or a stabilization on the particle number and location of the peaks included in this mode.

In the Aitken and accumulation modes, the peaks shift to larger diameters and a stabilization or even increase in number concentration is observed. For example, in E1, during $T_2$, the lognormal parameters were $D_3 = 52.1$ nm; $\sigma_3 = 0.80 \pm 0.09$ and $N_3 = 118 \pm 7$ cm$^{-3}$, while during $T_3$ they were $D_3 = 56.6$ nm; $\sigma_3 = 0.69 \pm 0.06$ and $N_3 = 143 \pm 5$ cm$^{-3}$. Concentrations registered prior to snowfall are recovered along events. Two possible explanations underlie this behaviour: it could be caused by changes in air masses (Babu et al., 2016) or by the resuspension of aerosol particles scavenged by snowflakes upon reaching the ground, returning to the atmosphere. Indeed, the resuspension is a very complex process that depends on several factors such as the solubility of the different aerosol species and the environmental conditions (Ariya et al., 2011; Pousse-Nottelmann et al., 2015).

Zikova and Zdimal (2016) in a rural background site (Kosêtice, Czech Republic) showed a PSD during snowfall seemingly with only one modal peak around 100 nm, while without snowflakes there was also a modal peak but located around 50 nm. Further, they observed an increment in

**Table 3**
Cations and anions concentration (μeq L$^{-1}$), pH, conductivity (μS cm$^{-1}$), *VWM* (Volume-weighted mean concentrations) and *W* scavenging coefficient for ionic species, registered in melted snow-water samples for E4, E5 and E6.

| Event | pH | Conductivity | $Na^+$ | $NH_4^+$ | $Mg^{+2}$ | $K^+$ | $Ca^{+2}$ | $F^-$ | $Cl^-$ | $SO_4^{2-}$ | $NO_3^-$ | $NO_2^-$ |
|---|---|---|---|---|---|---|---|---|---|---|---|---|
| E4 | 5.75 | 61.0 | BLD | BLD | 4.13 | 4.89 | 8.94 | BLD | 5.33 | 7.93 | 4.60 | BLD |
| E5 | 6.32 | 5.8 | 31.2 | BLD | 9.35 | 5.18 | 2.49 | BLD | 46.2 | 6.00 | 4.27 | BLD |
| E6 | 6.94 | 46.1 | 57.3 | 4.55 | 15.0 | 5.52 | 16.5 | 5.76 | 77.4 | 29.6 | 7.16 | BLD |
| *VWM* | – | – | 5.3 | 0.27 | 1.46 | 0.65 | 1.13 | 0.34 | 7.41 | 2.11 | 0.69 | – |
| *W* ($10^5$) | | | 34.6 | 5.3 | 57.8 | 24.5 | 18.5 | – | 31.8 | 18.7 | 15.57 | – |

BDL- below detection limit.

the concentration of aerosol larger than 200 nm during snowfall, a behaviour similar to that observed in some cases (E4 and E6) of our study. The lower number of modal peaks observed by Zikova and Zdimal (2016) during snowfalls is probably related to the location of the sampling point, a rural site without traffic emissions.

### 3.4. Chemical analysis of snow samples

The chemical composition of snow samples was analysed only for E4, E5 and E6 events (all of which had a North America air mass origin) due to operational issues in air samplers. E4 registered a WIOC concentration of 0.049 mg $L^{-1}$, a WIEC of 0.009 mg $L^{-1}$ and an WIOC/WIEC ratio of 5.3. The WIOC concentration was higher than that obtained in other studies of snow samples in mountain sites as in Cerqueira et al. (2010), who reported values of 0.096–1.400 μg $L^{-1}$ for Schauinsland (Germany) and 0.033–0.785 μg $L^{-1}$ for Sonnblick (Austria). However, the WIOC concentration was lower than those reported for Gdynia (Poland) by Witkowska and Lewandowska (2016) in a coastal urban environment, with values between 0.098 and 0.205 mg $L^{-1}$. With regard to other types of precipitation, similar values from 0.012 to 3.55 mg $L^{-1}$were obtained for rainwater in Nanchang (China) (Zou et al., 2020), while a lower value (0.0005 mg $L^{-1}$) was documented for Nam Co, Tibet (China) (Ming et al., 2010). The mist condition in Sao Paulo (Brazil) (Vasconcellos et al., 2018) showed higher WIOC values (1.5–4.9 mg $L^{-1}$). The WIEC was higher than the limits reported for snow samples in Gdynia (Poland) (0.003 and 0.004 mg $L^{-1}$) and within the limits obtained in Schauinsland (Germany) (0–0.192 mg $L^{-1}$) and Sonnblick (Austria) (0–0.12 mg $L^{-1}$) by Cerqueira et al. (2010). The WIOC and WIEC concentrations during E5 and E6 were below the detection limit (BLD).

DOC in snow samples showed concentrations of 0.51 mg $L^{-1}$ and 4.09 mg $L^{-1}$ during E4 and E5, respectively. It is worth stressing that E4 exhibited a higher insoluble and lower soluble carbon content than E5. E5 showed an effective scavenging between before and after snow, while E4 presented a great increment of particle concentration ($\%\Delta C_{global} = -164$ %). The reasons previously argued (change of air masses and/or resuspension of aerosols scavenged by snow) can be applied in this case. The low precipitation sampled during E6 did not allow the analysis of its DOC content.

The water-soluble inorganic ions in melted snow-water samples were also analysed in E4, E5 and E6 (Table 3). E6 presented the highest concentration of both cations and anions. While higher concentrations of $Na^+$, $Mg^{2+}$, $K^+$ and $Cl^-$ were obtained for E5, E4 presented higher levels of $Ca^{2+}$ and $SO_4^{2-}$.

The $PM_{10}$ concentrations before precipitation were 21.9, 16.3 and 18.1 μg $m^{-3}$, for E4, E5 and E6, respectively. In aerosol samples, OC and EC for these snowfalls accounted for 1.56, 1.35 and 1.51 μg OC $m^{-3}$ and 0.54, 0.38 and 0.36 μg EC $m^{-3}$, respectively. The concentrations of water-soluble inorganic ions the day before precipitation are included in Table A3. A clear relationship between $Ca^{2+}$, $SO_4^{2-}$ and $NO_3^-$ concentrations in aerosols before snowfall and the concentration registered in the melted snow-water samples was observed. This fact may indicate that these ions are scavenged regardless of snowfall characteristics. However, other ions such as $Na^+$, $NH_4^+$, $Mg^{2+}$, $K^+$ or $Cl^-$ did not show a proportional relationship between the pre-event concentration and that contained in the snow samples. Scavenging coefficient $W$ values for each ion indicated that $Mg^{2+}$, $Na^+$ and $Cl^-$ were scavenged more efficiently during snowfall, with higher values than those registered during rainfall events in the same sampling campaign (Oduber et al., 2021b). pH and conductivity mean values of melted snow-water samples were slightly higher than those obtained for rainfall samples (6.32 vs 6.20 and 37.6 vs 33.8 μS $cm^{-1}$).

## 4. Conclusions

A study about below cloud scavenging of snow has been conducted. Throughout the snowfalls, the scavenging coefficient showed fluctuations. An effective washing of particles was observed during the first 30 min of snowfall, while when analyzing the whole event (30 min before and 30 min after snowfall) an increase in particle number concentration (in all modes) was registered. This may be related to the facts that after the snowflakes fall to the ground and melt, the aerosol particles incorporated could return into the atmosphere and the arrival of air masses with a higher aerosol load after the snowfall. A different scavenging efficiency ($\%\Delta C$) and the scavenging coefficient ($\lambda$) values were obtained during the first 30 min: nucleation (36.3 ± 22.1 % and $3.02 \cdot 10^{-4} \pm 2.03 \cdot 10^{-4}$ $s^{-1}$), Aitken (30.4 ± 18.2 % and $2.37 \cdot 10^{-4} \pm 1.42 \cdot 10^{-4}$ $s^{-1}$) and accumulation (22.4 ± 17.3 % and $1.77 \cdot 10^{-4} \pm 1.42 \cdot 10^{-4}$ $s^{-1}$). The range of particle sizes that are less efficiently scavenged by snowfall was observed between 400 and 600 nm. The snowflake with the highest $\%\Delta C$ was that of 3 mm in size while the lowest was 6 mm, probably due to the lager number of hydrometeors for the 3 mm size. The particle size distributions were fitted to log-normal distributions and the parameters were compared before and after snow. In general, a decrease in concentration in all particle sizes was observed, except for some events, for which an increment was registered in aerosol size ranges higher than 200 nm. In the chemical composition of snow-water, the species with highest scavenging values were $Mg^{2+}$, $Na^+$ and $Cl^-$. A clear relationship between $Ca^{2+}$, $SO_4^{2-}$ and $NO_3^-$ concentrations before snow event and the concentration registered in the snow samples was noticed. This fact may indicate that these ions are scavenged regardless of snowfall characteristics.

The combination of SMPS and disdrometer measurements have made it possible to carry out a study about aerosol scavenging by snowflakes in the Mediterranean area, an information scarce in the literature. The estimation of the scavenging coefficients caused by several types of precipitation provide useful information on aerosol sinks to be used as input in climate models. Future studies will be focused on a high number of snow events with different snowfall intensities and the analysis of chemical composition changes.

The results obtained show that the scavenging caused by snowfall on aerosols at mid-latitudes is not as evident as in other works at high latitudes have documented, possibly related to the pollution level. It can be further analysed how much time is needed for pollution recovered its pre-snowfall level and how it is related to the environmental conditions.

## Fundings

This work was partially supported by the AERORAIN project (Ministry of Economy and Competitiveness, Grant CGL2014-52556-R, co-financed with FEDER funds), the University of León (Programa Propio 2018/00203/001), the AEROHEALTH project (Ministry of Science and Innovation, Grant PID2019-106164RB-I00, co-financed with European FEDER funds) and the Junta de Castilla y León (Grant LE025P20, co-financed with European FEDER funds) and the Spanish Ministry of Science, Innovation and Universities (Grant RTI2018-098189-B-I00). Furthermore, this publication is part of the project TED2021-132292B-I00, funded by MCIN/AEI/10.13039/501100011033 and by the European Union "NextGenerationEU"/PRTR. The financial support to CESAM by FCT/MCTES (UIDP/50017/2020+UIDB/50017/2020+ LA/P/0094/2020), through national funds, is also acknowledged.

## CRediT authorship contribution statement

**C. Blanco-Alegre:** Writing – original draft, Formal analysis, Investigation, Methodology, Writing – review & editing. **A.I. Calvo:** Funding acquisition, Methodology, Conceptualization, Writing – review & editing. **A. Castro:** Investigation, Methodology. **F. Oduber:** Investigation, Methodology. **E. Alonso-Blanco:** Investigation, Methodology, Writing – review & editing. **C. Alves:** Investigation, Methodology, Writing – review & editing. **M. Cerqueira:** Investigation, Methodology. **R. López:** Investigation, Methodology. **F. Lucarelli:** Investigation, Methodology. **S. Nava:** Investigation, Methodology. **G. Calzolai:** Investigation,

Methodology. **R. Fraile:** Funding acquisition, Methodology, Conceptualization, Writing – review & editing.

## Declaration of competing interest

The authors declare that they have no known competing financial interests or personal relationships that could have appeared to influence the work reported in this paper.

## Data availability

Data will be made available on request.

## Acknowledgements

The authors gratefully acknowledge the NOAA Air Resources Laboratory (ARL) for the provision of the HYSPLIT transport and dispersion model and/or READY website (http://www.ready.noaa.gov) for the provision of the ABL data used in this study.

## Appendix A

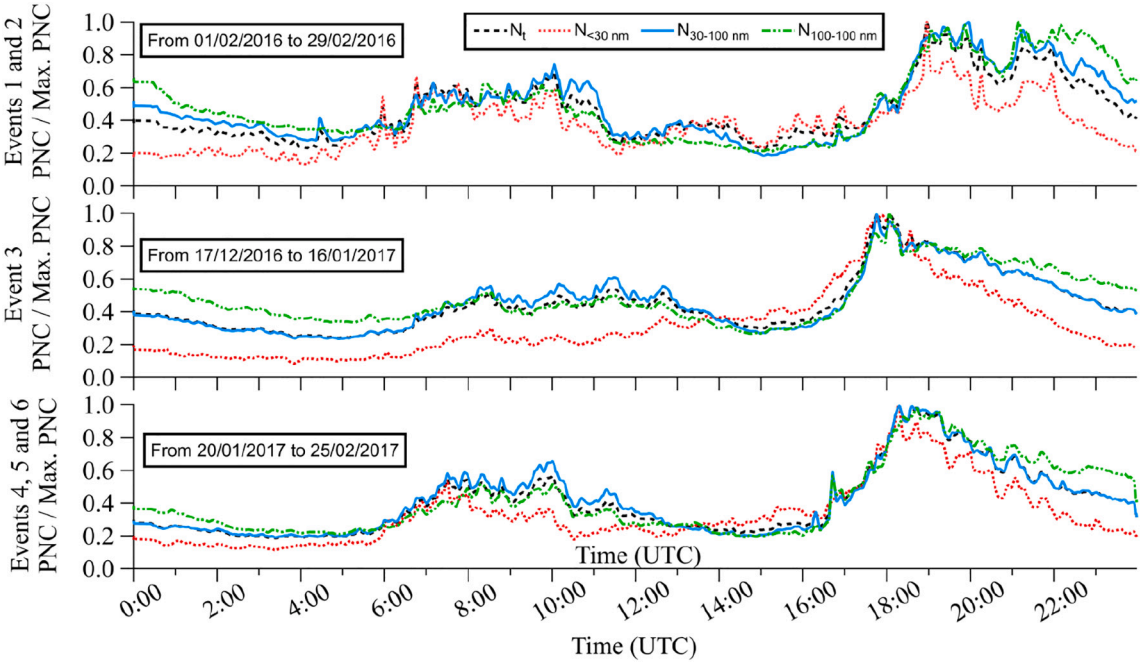


**Fig. A1.** Daily pattern of PNC by modes and total PNC represented as mean PNC/maximum mean PNC. The value obtained was applied to correct the PNC concentration registered every minute of each event.

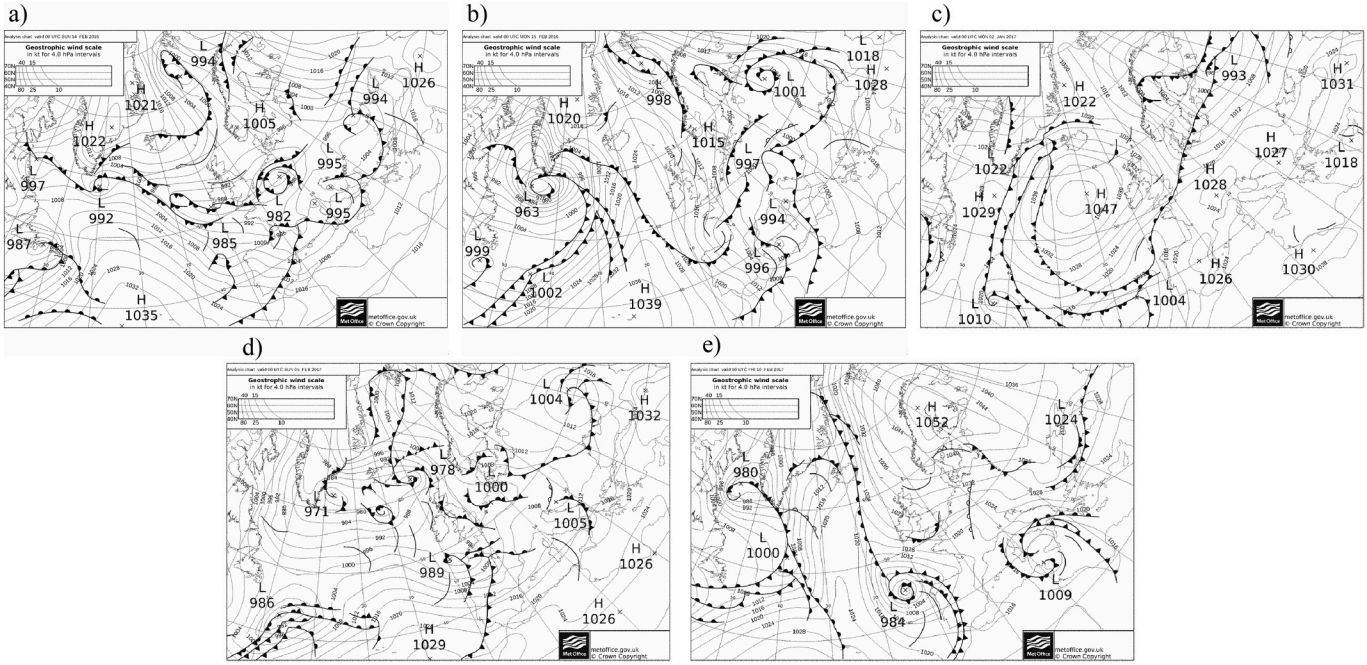

**Fig. A2.** Synoptic situation during snow events in León: a) E1; b) E2; c) E3; d) E4 and E5; and e) E6. Source: https://digital.nmla.metoffice.gov.uk/.

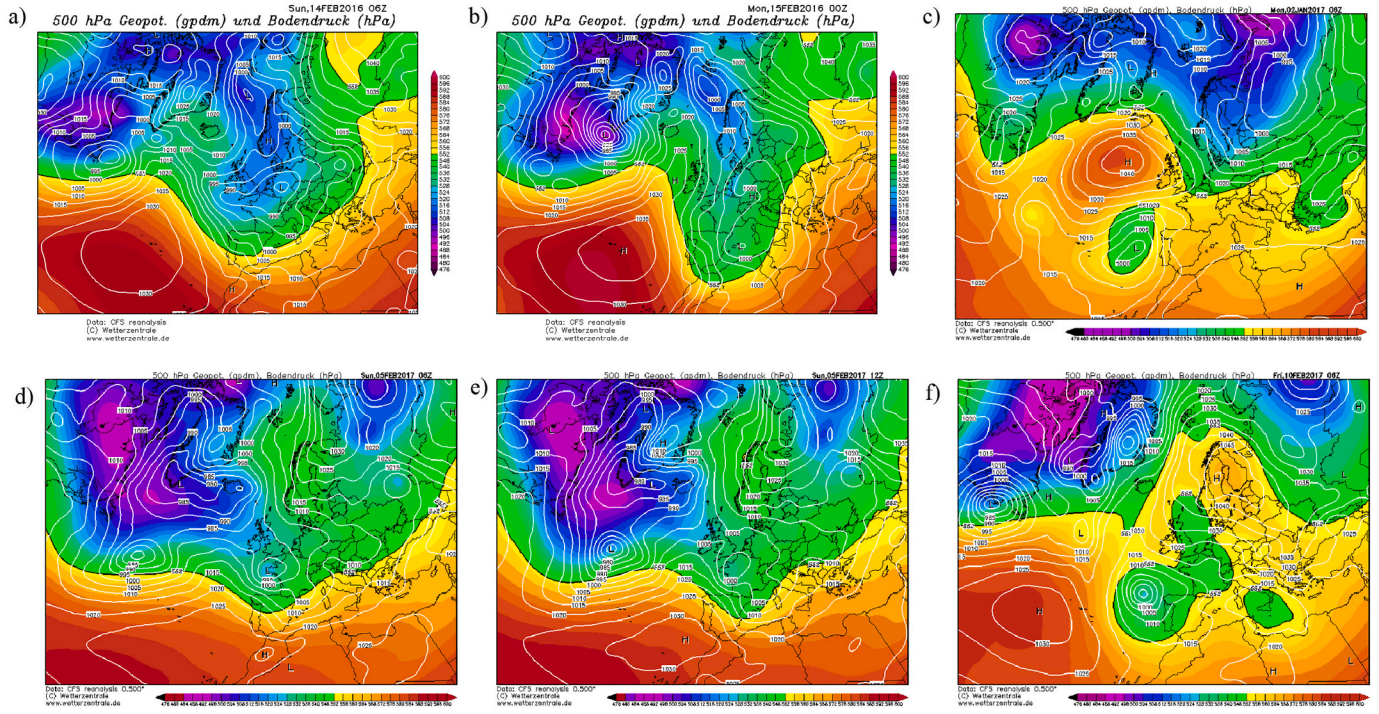


**Fig. A3.** Synoptic maps of surface pressure and geopotential altitude at 500 hPa during snow events in León: a) E1; b) E2; c) E3; d) E4 and E5; and e) E6. Source: www.wetterzentrale.de.

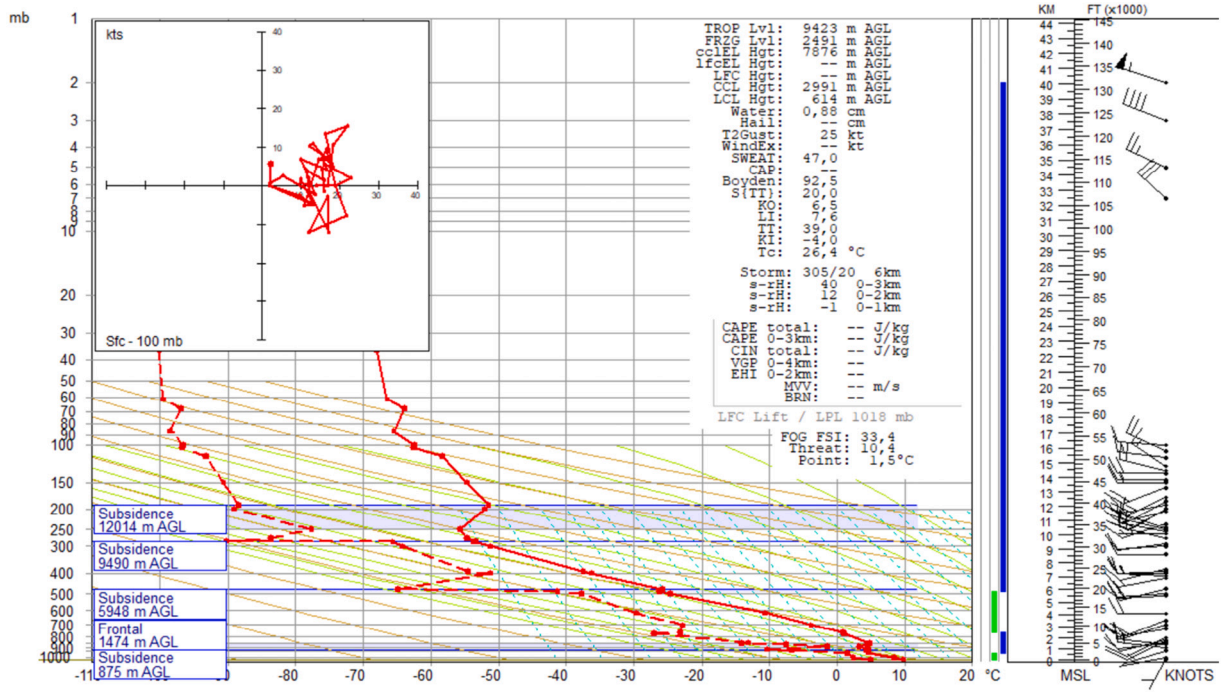


**Fig. A4.** Radiosonde available in Santander (Spain) the day 02/01/2017.

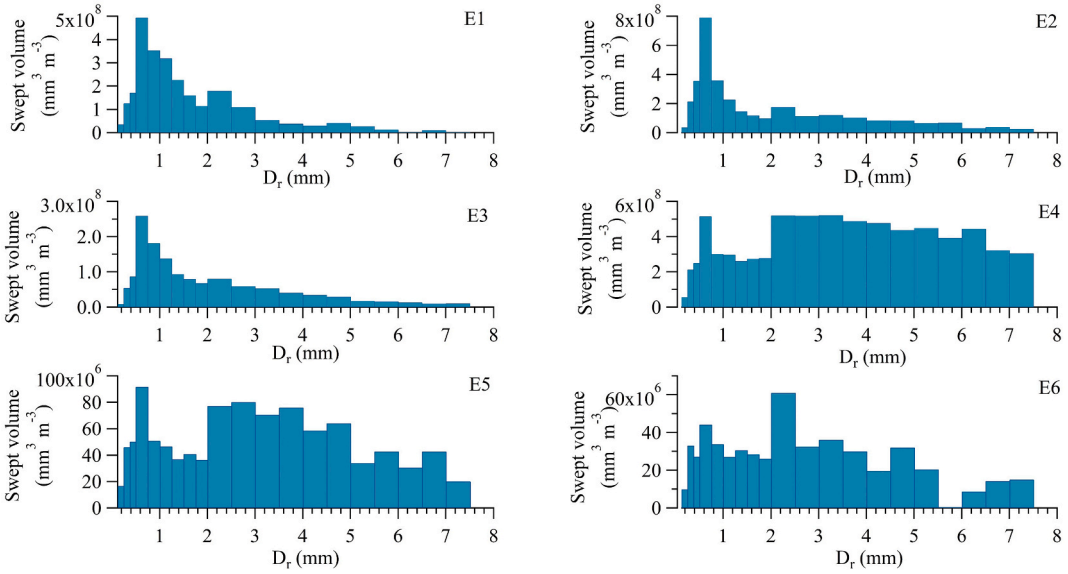


**Fig. A5.** Volume swept by snowflakes as a function of their size for each snowfall.

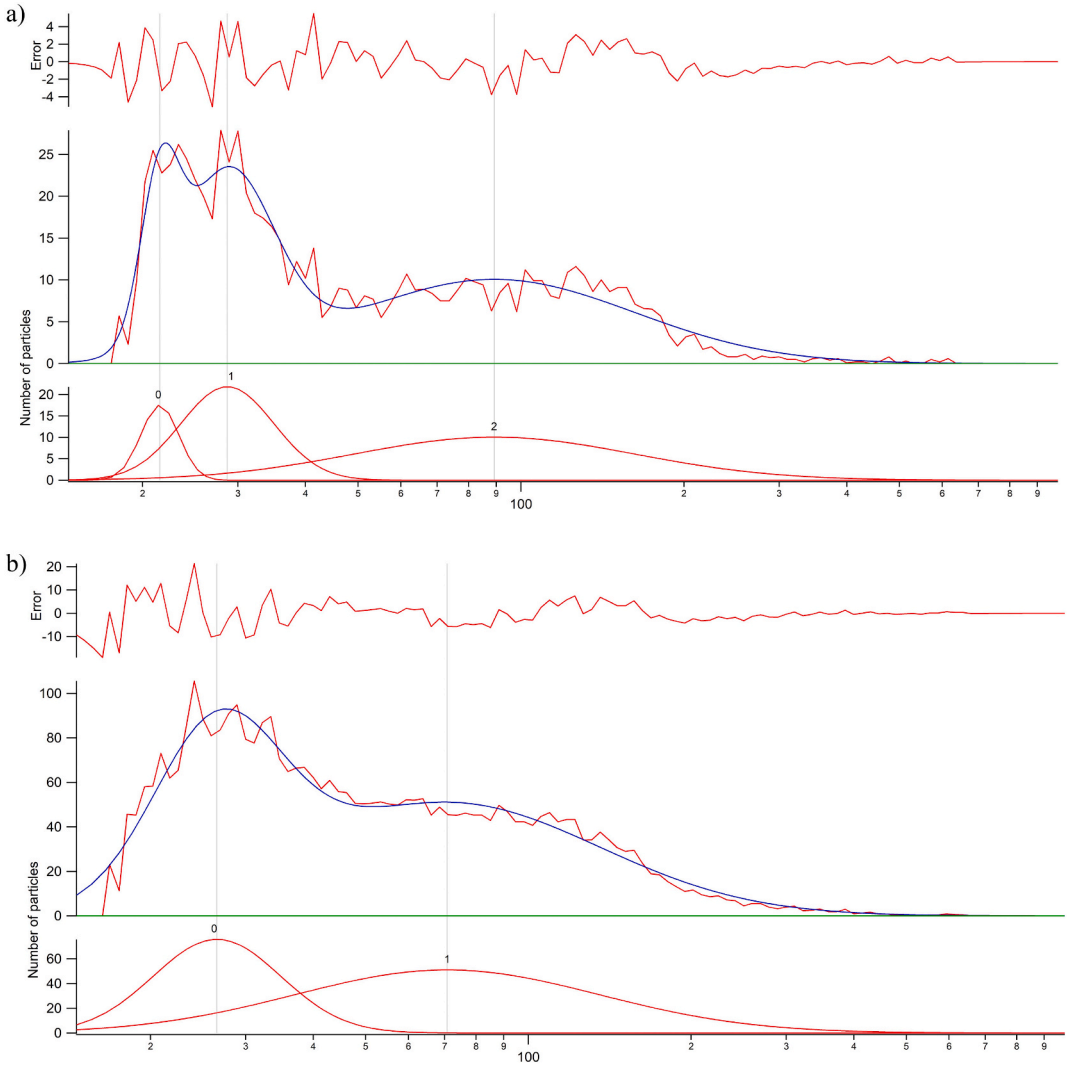


**Fig. A6.** Particle size distribution reconstructed of events 4 (a) and 5 (b), 30 min before snowfall start.

**Table A1**
For modes of nucleation (14–30 nm), Aitken (30–100 nm), accumulation (100–1000 nm) and global (14–1000 nm), mean PNC (corrected by daily pattern) before ($T_1$) and 30 min after precipitation ($T_4$), scavenging coefficient and scavenging efficiency ($\%\Delta C$).

| Event | $PNC_{nuc\ 1}$ ($cm^{-3}$) | $PNC_{nuc\ 4}$ ($cm^{-3}$) | $\lambda_{nuc}$ ($10^{-5}\ s^{-1}$) | $\%\Delta C_{nuc}$ | $PNC_{Ait\ 1}$ ($cm^{-3}$) | $PNC_{Ait\ 4}$ ($cm^{-3}$) | $\lambda_{Ait}$ ($10^{-5}\ s^{-1}$) | $\%\Delta C_{Ait}$ | $PNC_{acc\ 1}$ ($cm^{-3}$) | $PNC_{acc\ 4}$ ($cm^{-3}$) | $\lambda_{acc}$ ($10^{-5}\ s^{-1}$) | $\%\Delta C_{acc}$ | $PNC_{global1}$ ($cm^{-3}$) | $PNC_{global4}$ ($cm^{-3}$) | $\lambda_{global}$ ($10^{-5}\ s^{-1}$) | $\%\Delta C_{global}$ |
|---|---|---|---|---|---|---|---|---|---|---|---|---|---|---|---|---|
| E1 | 7885 | 1094 | 19.5 | 86.1 | 6191 | 874 | 19.3 | 85.9 | 1036 | 270 | 13.2 | 73.9 | 14,019 | 2083 | 18.8 | 85.1 |
| E2 | 3241 | 5839 | −1.2 | −80.1 | 1590 | 5858 | −2.6 | −268.4 | 428 | 1088 | −1.9 | −154 | 4306 | 11,880 | −2 | −175.9 |
| E3 | 619 | 1175 | −8.8 | −89.8 | 2997 | 3995 | −4 | −33.3 | 3794 | 4143 | −1.2 | −9.2 | 8611 | 9860 | −1.9 | −14.5 |
| E4 | 277 | 768 | −6 | −177.7 | 335 | 979 | −6.3 | −191.9 | 177 | 380 | −4.5 | −114.9 | 739 | 1948 | −5.7 | −163.8 |
| E5 | 1040 | 1021 | 2 | 1.9 | 1820 | 1813 | 0.4 | 0.4 | 721 | 683 | 0.2 | 0.2 | 3416 | 3381 | 1.1 | 1 |
| E6 | 3141 | 2978 | 0.9 | 5.2 | 5498 | 6842 | −3.8 | −24.4 | 1882 | 2808 | −6.9 | −49.2 | 10,056 | 12,289 | −3.4 | −22.2 |

**Table A2**
Mean values and standard deviation of lognormal aerosol particle size distributions during snow events before and after precipitation. $T_1$ = Before, $T_2$ = During first 30 min of precipitation and $T_3$ = During second 30 min of precipitation. $D$ is the diameter (nm), $N$ is the number of particles ($cm^{-3}$) and $\sigma$ is the width parameter.

| | Moment | $D_1$ | $N_1$ | $\sigma_1$ | $D_2$ | $N_2$ | $\sigma_2$ | $D_3$ | $N_3$ | $\sigma_3$ | $D_4$ | $N_4$ | $\sigma_4$ |
|---|---|---|---|---|---|---|---|---|---|---|---|---|---|
| E1 | $T_1$ | 21.0 ± 0.2 | 399 ± 99 | 0.01 ± 0.02 | 27.0 ± 1.0 | 454 ± 64 | 0.29 ± 0.06 | 49.1 ± 7.2 | 191 ± 22 | 0.74 ± 0.13 | | | |
| | $T_2$ | 20.9 ± 0.1 | 324 ± 39 | 0.09 ± 0.01 | 26.4 ± 0.6 | 276 ± 21 | 0.25 ± 0.03 | 52.1 ± 4.4 | 118 ± 7 | 0.80 ± 0.09 | | | |
| | $T_3$ | 21.3 ± 0.1 | 225 ± 39 | 0.11 ± 0.01 | 27.5 ± 0.9 | 182 ± 19 | 0.26 ± 0.05 | 56.6 ± 3.0 | 143 ± 5 | 0.69 ± 0.06 | | | |
| E2 | $T_1$ | 20.3 ± 0.2 | 228 ± 44 | 0.12 ± 0.02 | 25.3 ± 2.3 | 149 ± 13.9 | 0.48 ± 0.08 | | | | | | |
| | $T_2$ | 19.6 ± 0.1 | 155 ± 12 | 0.01 ± 0.01 | 25.7 ± 0.6 | 108 ± 5 | 0.33 ± 0.02 | | | | | | |
| | $T_3$ | 20.9 ± 0.0 | 252 ± 17 | 0.03 ± 0.01 | 25.2 ± 0.4 | 129 ± 6 | 0.40 ± 0.02 | | | | | | |
| E3 | $T_1$ | 17.1 ± 0.3 | 456 ± 394 | 0.01 ± 0.03 | 29.3 ± 0.9 | 50 ± 5 | 0.35 ± 0.04 | 115.7 ± 1.7 | 161 ± 3 | 0.79 ± 0.03 | | | |
| | $T_2$ | 30.3 ± 1.5 | 61 ± 9 | 0.30 ± 0.04 | 49.1 ± 9.7 | 15 ± 8 | 0.29 ± 0.21 | 122.2 ± 1.5 | 156 ± 1 | 0.75 ± 0.02 | | | |
| | $T_3$ | 59.6 ± 12.9 | 27 ± 5 | 1.56 ± 0.17 | 126.8 ± 1.6 | 138 ± 6 | 0.67 ± 0.02 | | | | | | |
| E4 | $T_1$ | 21.5 ± 0.1 | 18 ± 3 | 0.11 ± 0.02 | 28.7 ± 0.6 | 22 ± 1 | 0.28 ± 0.03 | 89.3 ± 3.5 | 10 ± 1 | 0.85 ± 0.06 | | | |
| | $T_2$ | 22.6 ± 0.1 | 13 ± 2 | 0.07 ± 0.01 | 30.1 ± 0.9 | 12 ± 1 | 0.51 ± 0.04 | 107.4 ± 3.5 | 10 ± 1 | 0.58 ± 0.05 | | | |
| | $T_3$ | 28.1 ± 0.4 | 13 ± 1 | 0.40 ± 0.02 | 96.5 ± 3.2 | 8 ± 1 | 0.77 ± 0.05 | | | | | | |
| E5 | $T_1$ | 20.9 ± 0.5 | 79 ± 44 | 0.29 ± 0.10 | 37.2 ± 10.8 | 19 ± 19 | 0.19 ± 0.41 | | | | | | |
| | $T_2$ | 25.7 ± 0.8 | 52 ± 20 | 0.31 ± 0.04 | 45.9 ± 5.7 | 44 ± 3 | 0.73 ± 0.27 | 133.1 ± 11.8 | 25 ± 6 | 0.40 ± 0.07 | | | |
| E6 | $T_1$ | 25.5 ± 0.3 | 67 ± 5 | 0.32 ± 0.03 | 62.5 ± 3.6 | 55 ± 2 | 0.99 ± 0.08 | 211.5 ± 22.6 | 4 ± 4 | 0.12 ± 0.16 | | | |
| | $T_2$ | 18.7 ± 0.2 | 25 ± 5 | 0.07 ± 0.02 | 26.0 ± 0.3 | 73 ± 2 | 0.32 ± 0.02 | 73.6 ± 0.7 | 115 ± 1 | 0.70 ± 0.02 | 268.8 ± 9.9 | 17 ± 2 | 0.36 ± 0.05 |
| | $T_3$ | 26.3 ± 0.6 | 99 ± 7 | 0.46 ± 0.02 | 69.7 ± 1.8 | 137 ± 2 | 0.72 ± 0.04 | 270.1 ± 20.7 | 15 ± 2 | 0.43 ± 0.10 | | | |

**Table A3**
Cations and anions concentration (μg $m^{-3}$) registered in 24-h sampled filters before snow events E4, E5 and E6.

| | $Na^+$ | $NH_4^+$ | $Mg^{+2}$ | $K^+$ | $Ca^{+2}$ | $F^-$ | $Cl^-$ | $SO_4^{2-}$ | $NO_3^-$ | $NO_2^-$ |
|---|---|---|---|---|---|---|---|---|---|---|
| Before E4 | 1.11 | 0.09 | 0.12 | 0.17 | 0.14 | BLD | 2.14 | 0.49 | 0.27 | BLD |
| Before E5 | 0.18 | 0.04 | 0.01 | 0.06 | 0.06 | BLD | 0.29 | 0.21 | 0.21 | BLD |
| Before E6 | 0.96 | 0.20 | 0.10 | 0.18 | 0.15 | BLD | 1.64 | 0.67 | 0.36 | BLD |

BDL- below detection limit.

## References


Alves, C.A., Lopes, D.J., Calvo, A.I., Evtyugina, M., Rocha, S., Nunes, T., 2015. Emissions from light-duty diesel and gasoline in-use vehicles measured on chassis dynamometer test cycles. Aerosol Air Qual. Res. 15, 99–116. https://doi.org/10.4209/aaqr.2014.01.0006.

Andronache, C., 2003. Estimated variability of below-cloud aerosol removal by rainfall for observed aerosol size distributions. Atmos. Chem. Phys. 3, 131–143. https://doi.org/10.5194/acp-3-131-2003.

Andronache, C., Grönholm, T., Laakso, L., Phillips, V., Venalainen, A., Phillips, Y., Venäläinen, A., 2006. Scavenging of ultrafine particles by rainfall at a boreal site: observations and model estimations. Atmos. Chem. Phys. 6, 4739–4754. https://doi.org/10.5194/acp-6-4739-2006.

Ariya, P.A., Domine, F., Kos, G., Amyot, M., Côté, V., Vali, H., Lauzier, T., Kuhs, W.F., Techmer, K., Heinrichs, T., Mortazavi, R., 2011. Snow - a photobiochemical

exchange platform for volatile and semi-volatile organic compounds with the atmosphere. Environ. Chem. 8, 62. https://doi.org/10.1071/EN10056.
Babu, S.S., Kompalli, S.K., Moorthy, K.K., 2016. Aerosol number size distributions over a coastal semi urban location: seasonal changes and ultrafine particle bursts. Sci. Total Environ. 563–564, 351–365. https://doi.org/10.1016/j.scitotenv.2016.03.246.
Bae, S.Y., Jung, C.H., Pyo Kim, Y., 2006. Development and evaluation of an expression for polydisperse particle scavenging coefficient for the below-cloud scavenging as a function of rain intensity using the moment method. J. Aerosol Sci. 37, 1507–1519. https://doi.org/10.1016/j.jaerosci.2006.02.003.
Battaglia, A., Rustemeier, E., Tokay, A., Blahak, U., Simmer, C., 2010. PARSIVEL snow observations: a critical assessment. J. Atmos. Ocean. Technol. 27, 333–344. https://doi.org/10.1175/2009JTECHA1332.1.
Blanco-Alegre, C., Castro, A., Calvo, A.I., Oduber, F., Alonso-Blanco, E., Fernández-González, D., Valencia-Barrera, R.M., Vega-Maray, A.M., Fraile, R., 2018. Below-cloud scavenging of fine and coarse aerosol particles by rain: the role of raindrop size. Q. J. R. Meteorol. Soc. 144, 2715–2726. https://doi.org/10.1002/qj.3399.
Blanco-Alegre, C., Calvo, A.I., Coz, E., Castro, A., Oduber, F., Prévôt, A.S.H.H., Močnik, G., Fraile, R., 2019. Quantification of source specific black carbon scavenging using an aethalometer and a disdrometer. Environ. Pollut. 246, 336–345. https://doi.org/10.1016/j.envpol.2018.11.102.
Blanco-Alegre, C., Calvo, A.I., Castro, A., Oduber, F., Alonso-Blanco, E., Fraile, R., 2021. Scavenging of submicron aerosol particles in a suburban atmosphere: the raindrop size factor. Environ. Pollut. 117371 https://doi.org/10.1016/j.envpol.2021.117371.
Blanco-Alegre, C., Calvo, A.I., Alonso-Blanco, E., Castro, A., Oduber, F., Fraile, R., 2022. Evolution of size-segregated aerosol concentration in NW Spain : a two-step classification to identify new particle formation events. J. Environ. Manag. 304, 114232. https://doi.org/10.1016/j.jenvman.2021.114232.
Cerqueira, M., Pio, C., Legrand, M., Puxbaum, H., Kasper-Giebl, A., Afonso, J., Preunkert, S., Gelencsér, A., Fialho, P., 2010. Particulate carbon in precipitation at European background sites. J. Aerosol Sci. 41, 51–61. https://doi.org/10.1016/j.jaerosci.2009.08.002.
Chate, D.M., Murugavel, P., Ali, K., Tiwari, S., Beig, G., 2011. Below-cloud rain scavenging of atmospheric aerosols for aerosol deposition models. Atmos. Res. 99, 528–536. https://doi.org/10.1016/j.atmosres.2010.12.010.
Croft, B., Lohmann, U., Martin, R.V., Stier, P., Wurzler, S., Feichter, J., Posselt, R., Ferrachat, S., 2009. Aerosol size-dependent below-cloud scavenging by rain and snow in the ECHAM5-HAM. Atmos. Chem. Phys. 9, 4653–4675. https://doi.org/10.5194/acp-9-4653-2009.
Custódio, D., Cerqueira, M., Fialho, P., Nunes, T., Pio, C., Henriques, D., 2014. Wet deposition of particulate carbon to the Central North Atlantic Ocean. Sci. Total Environ. 496, 92–99. https://doi.org/10.1016/j.scitotenv.2014.06.103.
Dockery, D.W., Sc, D., Stone, P.H., 2007. Cardiovascular risks from fine particulate air pollution. N. Engl. J. Med. 336, 511–513. https://doi.org/10.1056/NEJMe068274.
Draxler, R., Rolph, G., 2012. Hysplit (Hybrid Single-Particle Lagrangian Integrated Trajectory). Silver Spring. NOAA Air Resour, Lab.
Feng, J., 2009. A size-resolved model for below-cloud scavenging of aerosols by snowfall. J. Geophys. Res. Atmos. 114, 1–8. https://doi.org/10.1029/2008JD011012.
Franz, T.P., Eisenreich, S.J., 1998. Snow scavenging of polychlorinated biphenyls and polycyclic aromatic hydrocarbons in Minnesota. Environ. Sci. Technol. 32, 1771–1778. https://doi.org/10.1021/es970601z.
Fuzzi, S., Baltensperger, U., Carslaw, K., Decesari, S., Denier van der Gon, H., Facchini, M.C., Fowler, D., Koren, I., Langford, B., Lohmann, U., Nemitz, E., Pandis, S., Riipinen, I., Rudich, Y., Schaap, M., Slowik, J.G., Spracklen, D.V., Vignati, E., Wild, M., Williams, M., Gilardoni, S., 2015. Particulate matter, air quality and climate: lessons learned and future needs. Atmos. Chem. Phys. 15, 8217–8299. https://doi.org/10.5194/acp-15-8217-2015.
Greenfield, S.M., 1957. Rain scavenging of radioactive particulate matter from the atmosphere. J. Meteorol. https://doi.org/10.1175/1520-0469(1957)014<0115:RSORPM>2.0.CO;2.
Hussein, T., Karppinen, A., Kukkonen, J., Härkönen, J., Aalto, P., Hämeri, K., Kerminen, V.M., Kulmala, M., 2006. Meteorological dependence of size-fractionated number concentrations of urban aerosol particles. Atmos. Environ. 40, 1427–1440. https://doi.org/10.1016/j.atmosenv.2005.10.061.
Illuminati, S., Bau, S., Annibaldi, A., Mantini, C., Libani, G., Truzzi, C., Scarponi, G., 2016. Evolution of size-segregated aerosol mass concentration during the Antarctic summer at Northern Foothills, Victoria Land. Atmos. Environ. 125, 212–221. https://doi.org/10.1016/j.atmosenv.2015.11.015.
Jonasz, M., Fournier, G., 1996. Approximation of the size distribution of marine particles by a sum of log-normal functions. Limnol. Oceanogr. 41, 744–754. https://doi.org/10.4319/lo.1996.41.4.0744.
Jones, A.C., Hill, A., Hemmings, J., Lemaitre, P., Quérel, A., Ryder, C.L., Woodward, S., 2022. Below-cloud Scavenging of Aerosol by Rain : A Review of Numerical Modelling Approaches and Sensitivity Simulations With Mineral Dust 1–45.
Kang, S., Zhang, Y., Qian, Y., Wang, H., 2020. A review of black carbon in snow and ice and its impact on the cryosphere. Earth-Sci. Rev. 210, 103346. https://doi.org/10.1016/j.earscirev.2020.103346.
Kyrö, E.M., Grönholm, T., Vuollekoski, H., Virkkula, A., Kulmala, M., Laakso, L., 2009. Snow scavenging of ultrafine particles: field measurements and parameterization. Boreal Environ. Res. 14, 527–538.
Laakso, L., Grönholm, T., Rannik, Ü., Kosmale, M., Fiedler, V., Vehkamäki, H., Kulmala, M., 2003. Ultrafine particle scavenging coefficients calculated from 6 years field measurements. Atmos. Environ. 37, 3605–3613. https://doi.org/10.1016/S1352-2310(03)00326-1.
Ladino, L., Stetzer, O., Hattendorf, B., Günther, D., Croft, B., Lohmann, U., 2011. Experimental study of collection efficiencies between submicron aerosols and cloud droplets. J. Atmos. Sci. 68, 1853–1864. https://doi.org/10.1175/JAS-D-11-012.1.
Lei, Y.D., Wania, F., 2004. Is rain or snow a more efficient scavenger of organic chemicals? Atmos. Environ. 38, 3557–3571. https://doi.org/10.1016/j.atmosenv.2004.03.039.
Lemaitre, P., Sow, M., Quérel, A., Dépée, A., Monier, M., Menard, T., Flossmann, A., 2020. Contribution of phoretic and electrostatic effects to the collection efficiency of submicron aerosol particles by raindrops. Atmosphere (Basel) 11. https://doi.org/10.3390/atmos11101028.
Levin, Z., 2009. Aerosol Pollution Impact on Precipitation, Aerosol Pollution Impact on Precipitation. https://doi.org/10.1007/978-1-4020-8690-8.
Lucarelli, F., Chiari, M., Calzolai, G., Giannoni, M., Nava, S., Udisti, R., Severi, M., Querol, X., Amato, F., Alves, C., Eleftheriadis, K., 2015. The role of PIXE in the AIRUSE project “testing and development of air quality mitigation measures in Southern Europe”. Nucl. Instrum. Methods Phys. Res. Sect. B Beam Interact. Mater. Atoms 363, 92–98. https://doi.org/10.1016/j.nimb.2015.08.023.
Meyer, T., Wania, F., 2008. Organic contaminant amplification during snowmelt. Water Res. 42, 1847–1865. https://doi.org/10.1016/j.watres.2007.12.016.
Meyer, T., Wania, F., 2011. Modeling the elution of organic chemicals from a melting homogeneous snow pack. Water Res. 45, 3627–3637. https://doi.org/10.1016/j.watres.2011.04.011.
Ming, J., Xiao, C., Sun, J., Kang, S., Bonasoni, P., 2010. Carbonaceous particles in the atmosphere and precipitation of the Nam Co region, central Tibet. J. Environ. Sci. 22, 1748–1756. https://doi.org/10.1016/S1001-0742(09)60315-6.
Mitra, S.K., Vohl, O., Ahr, M., Pruppacher, H.R., 1990. A wind tunnel and theoretical study of the melting behavior of atmospheric ice particles. IV: experiment and theory for snow flakes. J. Atmos. Sci. 47, 584–591. https://doi.org/10.1175/1520-0469(1990)047<0584:AWTATS>2.0.CO;2.
Oduber, F., Calvo, A.I., Blanco-Alegre, C., Castro, A., Nunes, T., Alves, C., Sorribas, M., Fernández-González, D., Vega-Maray, A.M., Valencia-Barrera, R.M., Lucarelli, F., Nava, S., Calzolai, G., Alonso-Blanco, E., Fraile, B., Fialho, P., Coz, E., Prevot, A.S.H.H., Pont, V., Fraile, R., 2019. Unusual winter Saharan dust intrusions at Northwest Spain: air quality, radiative and health impacts. Sci. Total Environ. 669, 213–228. https://doi.org/10.1016/j.scitotenv.2019.02.305.
Oduber, F., Calvo, A.I., Blanco-Alegre, C., Castro, A., Alves, C., Cerqueira, M., Lucarelli, F., Nava, S., Calzolai, G., Martin-Villacorta, J., Esteves, V., Fraile, R., 2021a. Towards a model for aerosol removal by rain scavenging: the role of physical-chemical characteristics of raindrops. Water Res. 190, 1–5. https://doi.org/10.1016/j.watres.2020.116758.
Oduber, F., Calvo, A.I., Castro, A., Blanco-Alegre, C., Alves, C., Calzolai, G., Nava, S., Lucarelli, F., Nunes, T., Barata, J., Fraile, R., 2021b. Characterization of aerosol sources in León (Spain) using Positive Matrix Factorization and weather types. Sci. Total Environ. 754, 142045. https://doi.org/10.1016/j.scitotenv.2020.142045.
Paramonov, M., Grönholm, T., Virkkula, A., 2011. Below-cloud scavenging of aerosol particles by snow at an urban site in Finland. Boreal Environ. Res. 16, 304–320. https://doi.org/10.1017/CBO9781107415324.004.
Pio, C., Cerqueira, M., Harrison, R.M., Nunes, T., Mirante, F., Alves, C., Oliveira, C., Sanchez, A., Campa, D., Artíñano, B., Matos, M., 2011. OC / EC ratio observations in Europe : re-thinking the approach for apportionment between primary and secondary organic carbon. Atmos. Environ. 45, 6121–6132. https://doi.org/10.1016/j.atmosenv.2011.08.045.
Pousse-Nottelmann, S., Zubler, E.M., Lohmann, U., 2015. Microphysical processing of aerosol particles in orographic clouds. Atmos. Chem. Phys. 15, 9217–9236. https://doi.org/10.5194/acp-15-9217-2015.
Pryor, S.C., Joerger, V.M., Sullivan, R.C., 2016. Empirical estimates of size-resolved precipitation scavenging coefficients for ultrafine particles. Atmos. Environ. 143, 133–138. https://doi.org/10.1016/j.atmosenv.2016.08.036.
Radke, L.F., Hobbs, P.V., Eltgroth, M.W., 1980. Scavenging of aerosol particles by precipitation. J. Appl. Meteorol. https://doi.org/10.1175/1520-0450(1980)019<0715:SOAPBP>2.0.CO;2.
Rosenfeld, D., Andreae, M.O., Asmi, A., Chin, M., de Leeuw, G., Donovan, D.P., Kahn, R., Kinne, S., Kivekäs, N., Kulmala, M., Lau, W., Schmidt, K.S., Suni, T., Wagner, T., Wild, M., Quaas, J., 2014. Global observations of aerosol-cloud-precipitation-climate interactions. Rev. Geophys. 52, 750–808. https://doi.org/10.1002/2013RG000441.
Russo, A., Sousa, P.M., Durão, R.M., Ramos, A.M., Salvador, P., Linares, C., Díaz, J., Trigo, R.M., 2020. Saharan dust intrusions in the Iberian Peninsula: predominant synoptic conditions. Sci. Total Environ. 717, 137041. https://doi.org/10.1016/j.scitotenv.2020.137041.
Ryu, Y.H., Min, S.K., 2022. Improving wet and dry deposition of aerosols in WRF-Chem: updates to below-cloud scavenging and coarse-particle dry deposition. J. Adv. Model. Earth Syst. 14 https://doi.org/10.1029/2021MS002792.
Seinfeld, J.H., Pandis, S.N., 2016. Atmospheric Chemistry and Physics: From Air Pollution to Climate Change, Atmospheric Chemistry and Physics. Wiley. https://doi.org/10.1016/0016-7037(87)90252-3.
Slinn, W.G.N., 1983. Precipitation Scavenging. Division of Biomedical Environmental Research. US Department of Energy, Washington DC.
Su, T., Li, Z., Kahn, R., 2018. Relationships between the planetary boundary layer height and surface pollutants derived from lidar observations over China: regional pattern and influencing factors. Atmos. Chem. Phys. 18, 15921–15935. https://doi.org/10.5194/acp-18-15921-2018.
Tang, G., Zhao, P., Wang, Yinghong, Gao, W., Cheng, M., Xin, J., Li, X., Wang, Yuesi, 2017. Mortality and air pollution in Beijing: the long-term relationship. Atmos. Environ. 150, 238–243. https://doi.org/10.1016/j.atmosenv.2016.11.045.
UNICEF, 2016. Clear the Air for Children (The impact of air pollution on children).
Vasconcellos, P.C., Gonçalves, F.L.T., Avila, S.G., Censon, V.K., Bauer, H., 2018. The chemical composition of winter fogs at são paulo highway sites. J. Braz. Chem. Soc. 29, 1951–1958. https://doi.org/10.21577/0103-5053.20180072.

Wiedensohler, A., Birmili, W., Nowak, A., Sonntag, A., Weinhold, K., Merkel, M., Wehner, B., Tuch, T., Pfeifer, S., Fiebig, M., Fjäraa, A.M., Asmi, E., Sellegri, K., Depuy, R., Venzac, H., Villani, P., Laj, P., Aalto, P., Ogren, J.A., Swietlicki, E., Williams, P., Roldin, P., Quincey, P., Hüglin, C., Fierz-Schmidhauser, R., Gysel, M., Weingartner, E., Riccobono, F., Santos, S., Grüning, C., Faloon, K., Beddows, D., Harrison, R., Monahan, C., Jennings, S.G., O'Dowd, C.D., Marinoni, A., Horn, H.G., Keck, L., Jiang, J., Scheckman, J., McMurry, P.H., Deng, Z., Zhao, C.S., Moerman, M., Henzing, B., De Leeuw, G., Löschau, G., Bastian, S., 2012. Mobility particle size spectrometers: harmonization of technical standards and data structure to facilitate high quality long-term observations of atmospheric particle number size distributions. Atmos. Meas. Tech. 5, 657–685. https://doi.org/10.5194/amt-5-657-2012.

Witkowska, A., Lewandowska, A.U., 2016. Water soluble organic carbon in aerosols (PM1, PM2.5, PM10) and various precipitation forms (rain, snow, mixed) over the southern Baltic Sea station. Sci. Total Environ. 573, 337–346. https://doi.org/10.1016/j.scitotenv.2016.08.123.

Witkowska, A., Lewandowska, A., Falkowska, L.M., 2015. Parallel measurements of organic and elemental carbon dry (PM1, PM2.5) and wet (rain, snow, mixed) deposition into the Baltic Sea. Mar. Pollut. Bull. 104, 1–10. https://doi.org/10.1016/j.marpolbul.2016.01.003.

Zhao, S., Yu, Y., He, J., Yin, D., Wang, B., 2015. Below-cloud scavenging of aerosol particles by precipitation in a typical valley city, northwestern China. Atmos. Environ. 102, 70–78. https://doi.org/10.1016/j.atmosenv.2014.11.051.

Zikova, N., Zdimal, V., 2016. Precipitation scavenging of aerosol particles at a rural site in the Czech Republic. Tellus B 68, 1–14. https://doi.org/10.3402/tellusb.v68.27343.

Zou, C., Zhang, Y., Gao, Y., Mao, X., Huang, H., Tan, Y., 2020. Characteristics, distribution, and sources of particulate carbon in rainfall collected by a sequential sampler in Nanchang, China. Atmos. Environ. 235, 117619. https://doi.org/10.1016/j.atmosenv.2020.117619.